CONSTRUCTION OF A SCANNING TUNNELING MICROSCOPE FOR IMAGING OF CARBON NANOTUBES

by

MATTHEW DAVID ELLIS, B.S.Engr.Physics

A THESIS

IN

APPLIED PHYSICS

Submitted to the Graduate Faculty
of Texas Tech University in
Partial Fulfillment of
the Requirements for
the Degree of

MASTER OF SCIENCE

Approved

Accepted

Dean of the Graduate School

May, 1998

TABLE OF CONTENTS

ABSTRACT

Scanning tunneling microscopy has become a widely used technique for surface science. This paper begins with an overview of the scanning tunneling microscope (STM) and then discusses in more detail the concepts of atomic scale tunneling and the image forming mechanism in a scanning tunneling microscope. The design and construction of a STM is then presented with an examination of the design parameters. This paper finishes with a brief look at carbon nanotubes and the imaging of these nanotubes with the STM.

LIST OF FIGURES

CHAPTER I

INTRODUCTION

Invented in 1982 by Binnig and Rohrer,[1] the scanning tunneling microscope (STM) was the first instrument to perform real space atomic resolution imaging of the surface of a material. The first success of this instrument was to resolve the debate concerning the surface reconstruction of the Si(111) surface.[2] Since then, the STM has become a very powerful tool for surface science. The success of the STM spawned an entire class of scanning probe microscopes and corresponding techniques. Scanning force microscopes such as the magnetic force microscope (MFM), the electrostatic force microscope (EFM), and the atomic force microscope (AFM), have been developed based on the STM. Many techniques such as scanning capacitance microscopy, scanning Kelvin microscopy, and scanning tunneling spectroscopy are now routinely employed via scanning probe microscopes for surface science.

Historical Development

The topografiner was the earliest instrument to resemble the STM in functionality. Using a piezoelectric drive system similar to the STM, this instrument scanned surfaces to obtain an image. Instead of using a tunneling current through a small potential barrier as the sensing mechanism, the topografiner used field emission for the electron source. Developed in the late 1960s by Young, Ward, and Scire, the topografiner scanned with the probe about 1000 Å from the surface. Applying a high voltage of a few kV created a

field emission current. Using the field emission current intensity as the feedback signal created topographic images of the sample. The lateral resolution of this device was at best approximately 4000 Å. Young also used the topografiner to study vacuum tunneling. Early work in vacuum tunneling provided the theoretical basis for understanding the tunneling mechanism in scanning tunneling microscopy.

Operating Mechanism

The scanning tunneling microscope is essentially a very sensitive profilometer that uses quantum mechanical tunneling as the sensing method. A small metallic probe, usually made of tungsten or a platinum-iridium alloy, is scanned across a sample surface by piezoelectric transducers (Figure 1). These transducers provide motion in three

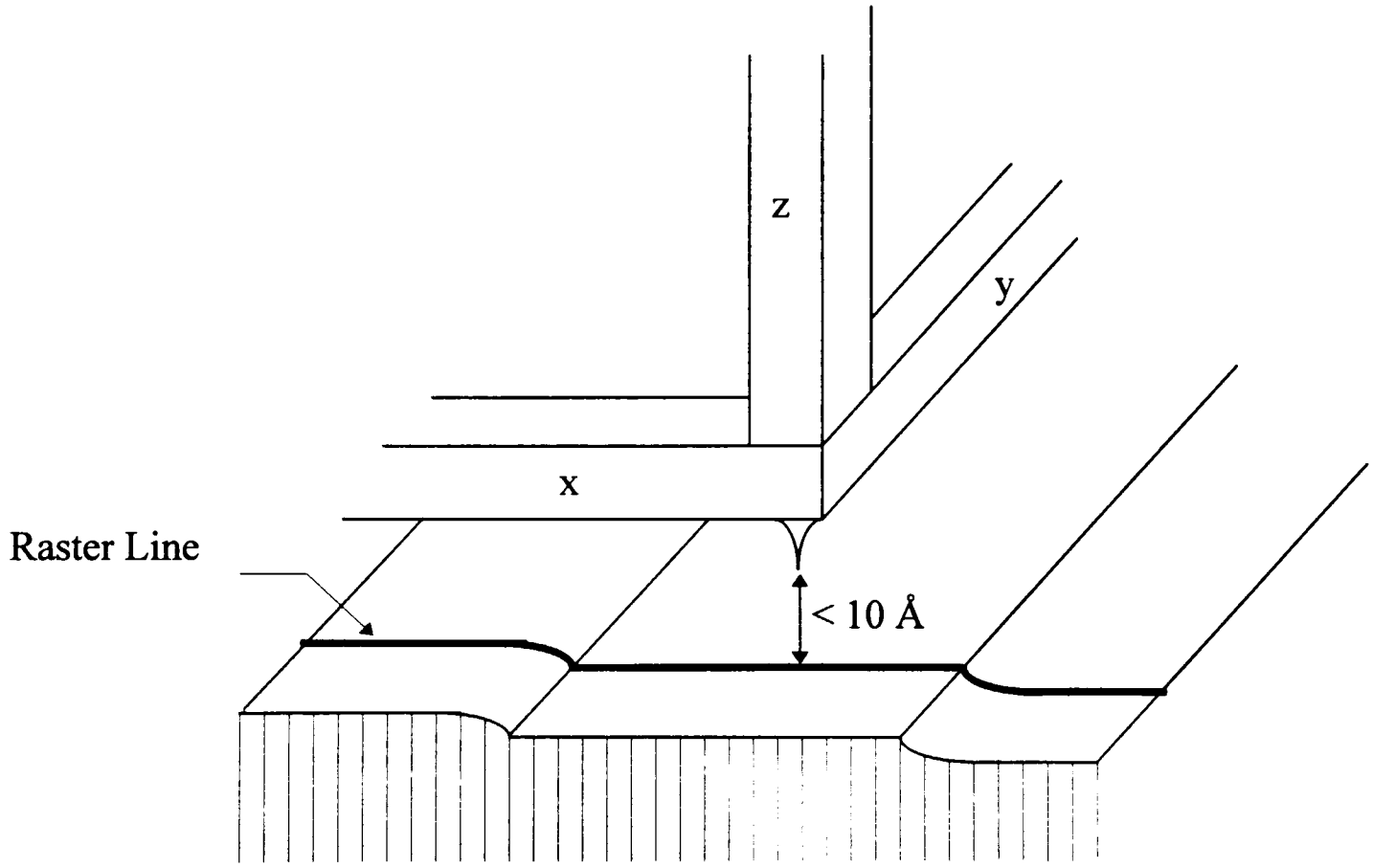

Figure 1. STM Principle of Operation

orthogonal directions. A saw tooth waveform rasters the probe in the x-direction, while a ramp voltage advances the raster signal in the y-direction. With this notation the probe-sample distance is on the z-axis. A third voltage adjusts this z distance so that the probe and sample remain separated by a few angstroms creating a small vacuum potential barrier.

Scanning a metal probe a few angstroms from a surface is usually impossible without some type of feedback and control system. A tunneling current across the vacuum barrier provides the input for such a feedback and control system. By overlapping the electron wavefunctions in the metallic probe and the sample, tunneling current flows when a bias is applied between the probe and sample. Amplifying this tunneling current and comparing it to a set point value creates a signal suitable for feedback on the voltage applied to the z piezoelectric transducer. This feedback loop created by the tunneling current and the z piezoelectric transducer voltage maintains a constant separation distance between the probe and the sample as scanning occurs, creating an array of z voltages that represent a contour plot of the sample.

Tunneling

Tunneling, a quantum mechanical phenomenon, creates the high degree of sensitivity necessary for atomic scale imaging of surfaces. Since the scanning tunneling microscope works by measuring the tunneling current between a sharp metal probe and a sample surface, a very simple model of vacuum tunneling between two metals can explain why the scanning tunneling microscope is so sensitive.

The standard one-dimensional square barrier problem in quantum mechanics shows the exponential current dependence on the probe-sample separation. Figure 2 shows a square energy barrier in one dimension with an electron wave packet originating

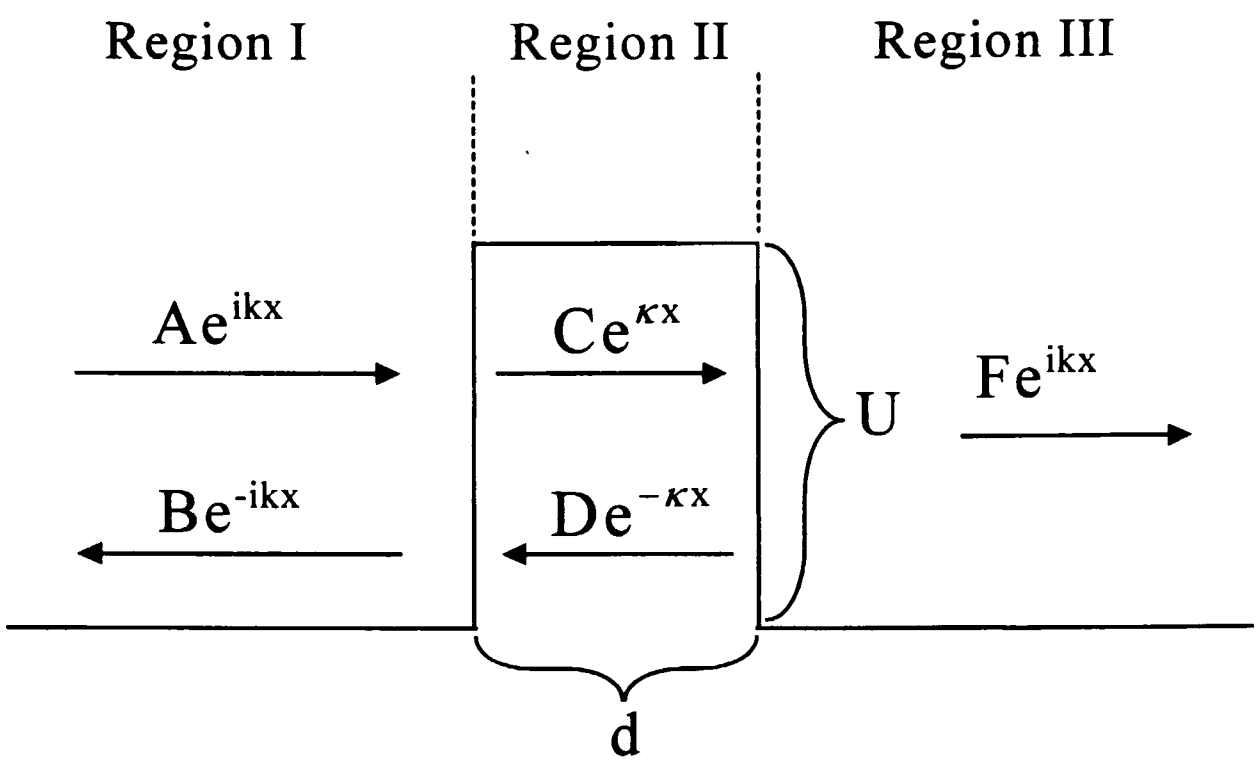

Figure 2. Square barrier of width d and height U

from the left side of the barrier. The width of this barrier, d, roughly corresponds to the separation between the probe and sample. The barrier height, U, depends on many factors and is difficult to determine. In general, the Schrödinger equation for this situation is as follows:

$$\frac{p_x^{\,2}}{2m} + U(x) = E \tag{1}$$

$$-\frac{\hbar^2}{2m}\frac{\partial^2}{\partial x^2}\psi(x) + U(x)\psi(x) = E\psi(x). \tag{2}$$

Assuming the solution to equation 2 is of exponential form results in two cases. The first case, when the energy of the particle is greater than the barrier energy, we have an oscillating solution of the form:

$$\psi(x) = \psi(0)e^{\pm ikx} \tag{3}$$

$$k = \frac{\sqrt{2m(E-U)}}{\hbar}. \tag{4}$$

The second case deals with the operational mode of the STM. In this situation, the energy of the particle is less than the energy of the barrier and the solutions are of the form:

$$\psi(x) = \psi(0)e^{-\kappa x} \tag{5}$$

$$\kappa = \frac{\sqrt{2m(U-E)}}{\hbar}. \tag{6}$$

From this solution, we can determine the probability for an electron crossing the barrier

$$P \propto \left|\psi_n(0)\right|^2 e^{-2\kappa x} \tag{7}$$

$$I \propto e^{-2\kappa d} \tag{8}$$

and find that the current is exponentially dependent on the distance between the probe and the sample.

Equation 8 shows that the tunneling current, I, is proportional to the exponential of the separation distance d. The decay constant, κ, is proportional the square root of the difference between the barrier energy U and the electron energy E. The energy E is the energy of electrons in the Fermi level neglecting thermal excitation. The difference of U and E can be described as the work function φ. For many metals, the work function is

approximately 4-5 eV, which makes the factor of 2κ approximately equal to 2Å^{-1}. Therefore, the tunneling current changes by almost an order of magnitude for every angstrom of vacuum between the electrodes. This extreme current sensitivity provides the basic means of measuring the sample surface.

Constant Height and Constant Current Imaging

As mentioned previously, to obtain a surface image the probe is scanned across the surface with feedback creating what is known as a "constant current" scan. For atomically smooth surfaces, the probe may be scanned across the surface with very slow feedback, allowing the tunneling current variations to determine the surface topography. This method is known as the "constant height" scan. Each method of obtaining images has advantages and disadvantages. Constant height scanning works well when slowly imaging small areas with small height variations. Problems with this approach stem from the inability to prevent the probe from crashing into large surface features on the sample. Constant current imaging can overcome this problem in many instances. Feedback from the tunneling current maintains a safe distance from the sample, allowing for fast scans over a rough surface. In either case, keeping a small metal probe within angstroms of a surface is a difficult problem with many challenges.

CHAPTER II

ATOMIC SCALE TUNNELING AND IMAGING

The physical interaction used in obtaining the surface information for a scanning tunneling microscope is quantum mechanical tunneling. A brief and simplified discussion of tunneling through a vacuum barrier was given above. Now a more detailed examination of the tunneling mechanism follows. The simplest explanation of the scanning tunneling microscope as a very sensitive profilometer depends on the belief that at the atomic scale the STM is actually taking a surface profile of the sample. At an atomic scale the notion of surface topography is unclear. A simple assumption would be that surface topography at the atomic scale is a contour of the charge density of the surface material. Only electrons near the Fermi level contribute to the tunneling and all electrons below the Fermi level contribute to the charge density, so, assuming that the topography produced by changes in the tunneling current is a contour of the charge density may not be entirely correct.[3]

In addition to the uncertainty regarding the surface topography, the electron transport processes in an STM are different from the standard mechanism described as tunneling. Usually, the tunneling process has a barrier width of 20-30 angstroms; but in an STM, the barrier is only a few angstroms wide. Also, overlap between the surface potentials of the probe and sample may place the top of the potential barrier lower than that of the vacuum level.[4] Sometimes the potential barrier level is even lower than the Fermi level. The local atomic structure between the probe and the sample also plays an

important role in determining the current. Finally, many forces exist between the probe and the sample affecting the tunneling current.

Ballistic Transport and Tunneling

Atomic scale tunneling differs from conventional tunneling in one important aspect. The width of the potential barrier is small compared to that in usual discussions of tunneling. In fact, with a small enough barrier tunneling might not be an accurate description of the process occurring. Arguments invoking the uncertainty principle show that the location of the electron is unknown with respect to the barrier.[5] Thus, regarding atomic scale potential barriers the difference between ballistic transport and tunneling is nonexistent. Two approaches with the uncertainty principle show this nondistinction.

The first approach shows the uncertainty of the electron energy, in the region of the barrier, is greater than its kinetic energy. Inside the region of the barrier, the electron has a velocity determined by its kinetic energy.

$$v = \sqrt{\frac{2(E - U_B)}{m}} \tag{9}$$

With this velocity, the time for an electron to pass through the barrier is:

$$\Delta t = d\sqrt{\frac{m}{2(E - U_B)}}\,. \tag{10}$$

Using the energy-time uncertainty relation:

$$\Delta E \geq \frac{\hbar}{\Delta t} = \frac{\hbar}{d}\sqrt{\frac{2(E - U_B)}{m}}\,. \tag{11}$$

Assuming $E - U_B = 3$ eV, and the barrier thickness is approximately 2 Å, the energy uncertainty, ΔE, is about 3.4 eV. Thus, the uncertainty of the energy is larger than the absolute value of the electron kinetic energy.

The second approach shows the uncertainty in position of an electron may be greater than the barrier thickness. The de Broglie wavelength of the electron in the classically allowed region of the barrier is given by equation 12.

$$\lambda = \frac{2m\hbar}{\sqrt{2m(E - U_B)}} \tag{12}$$

Given an electron with a kinetic energy of 3 eV, the de Broglie wavelength of the electron is approximately 7.1 Å, which is the same order of magnitude as the barrier thickness.

Modeling the Tunneling Current

Regardless of the uncertainty relations given above, a tunneling Hamiltonian approach using first order perturbation theory may be used to calculate the tunneling current. Based on a method developed by Bardeen[6] for metal-insulator-metal tunneling junctions, this approach begins by considering two subsystems instead of attempting to analyze the Schrödinger equation of the combined system. For each subsystem, solving the stationary Schrödinger equation determines the electronic states. Then, using time dependent perturbation theory, the electron transfer rate between the electrodes may be found. The overlap of the surface wavefunctions of the two subsystems at a separation surface determines the amplitude of the electron transfer, also known as the tunneling matrix M. By modifying the wavefunctions of one surface due to the presence of the

other, the Bardeen approach to tunneling may be applied to tunneling in an STM. This method is also known as the modified Bardeen approach (MBA).[7]

Using this approach, the tunneling current is,

$$I = \frac{2me}{\hbar} \sum_{\mu,\nu} \left\{ f(E_\mu)\left[1 - f(E_\nu)\right] - f(E_\nu)\left[1 - f(E_\mu)\right] \right\} \left| M_{\mu\nu} \right|^2 \delta(E_\nu + V - E_\nu). \quad (13)$$

In this expression, *f(E)* is the Fermi function, V is the applied voltage, and $M_{\mu\nu}$ is the tunneling matrix element between the state of the probe and the sample. Evaluating the tunneling matrix $M_{\mu\nu}$ is usually the most difficult step in determining the tunneling current. This difficulty stems from lack of knowledge of the probe and sample wavefunctions. If the probe and sample wavefunctions are known, $M_{\mu\nu}$ can be evaluated using the expression developed by Bardeen

$$M_{\mu\nu} = -\frac{\hbar^2}{2m} \int_{\Sigma} \left(\chi_\nu^* \nabla \psi_\mu - \psi_\mu \nabla \chi_\nu^* \right) \bullet dS. \quad (14)$$

Equation 14 determines the tunneling matrix $M_{\mu\nu}$. In this expression, χ_ν is the modified wavefunction for the probe and ψ_μ is the wavefunction for the sample. The integral is performed over the surface area defined by S.

Local Density of States (LDOS) Topography

Although the MBA model works reasonably well for a variety of conditions, this model requires knowledge of the wavefunction of the surface and the probe. As mentioned previously, these wavefunctions are usually not known, especially for the tunneling probe. Assuming a simple model for the probe, and using the first order

perturbation theory for determining the tunneling current, leads to the conclusion that the tunneling current is proportional to the local density of states.

The simplest model of the probe is that it is a point source of current. Assuming the probe is a point source of current allows the analysis to determine properties of the sample only. In actual STM measurements, the probe and sample wavefunctions are responsible for the tunneling current. With the probe modeled as a mathematical point source of current, equation 13 for the current at small voltages reduces to[8]

$$I \propto \sum_{\nu} |\psi_{\mu}(r)|^2 \delta(E_{\mu} - E_F) \equiv \rho(r, E_F). \tag{15}$$

In this equation, E_F is the Fermi level of the sample surface, ψ_{μ} is the wavefunction for the surface at position r. The quantity $\rho(r,E_F)$ is the local density of states of the sample.

Lateral Resolution Models

Initial attempts to estimate the resolution of a scanning tunneling microscope showed that a very high resolution was possible with even a moderately sharp probe. The initial spherical probe model by Binnig, the s-wave model, and probe-sample interactions provide insight to the origin of atomic resolution in the scanning tunneling microscope.

One of the first estimates of the lateral resolution of the STM came from Binnig in 1978.[9] Assuming the tunneling probe was spherical in shape with a radius R, Binnig determined the tunneling current would be related to the probe radius by equation 16.

$$I(\Delta x) = I_0 e^{\left(-2\kappa \frac{\Delta x^2}{2R}\right)} \tag{16}$$

This equation is based on the idea that the probe radius is much larger than the distance between the probe and the surface. In this case, the current lines are almost perpendicular to the sample surface (Figure 3).

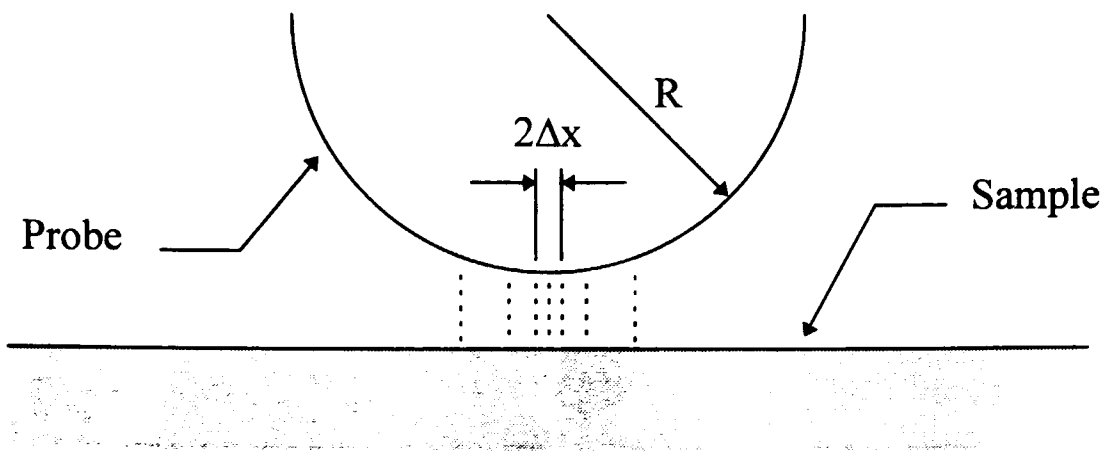

Figure 3. Current From a Spherical Probe

With $\kappa \approx 1$ Å^{-1} and R≈100 Å, the current concentrates in a small radius of approximately 14 Å; thus, the expected resolution should not exceed this value. Modern scanning tunneling microscopes routinely exceed this resolution. Thus, a more accurate model of the probe-sample interaction is necessary.

Soon after achieving atomic resolution with the STM, Tersoff and Hamann[10] proposed the s-wave model of probe sample interaction to account for the experimental results of Binnig and Rohrer. They modeled the probe as a protruded piece of Sommerfeld metal with a radius of curvature of R (Figure 4). The probe wavefunctions were then assumed to be solutions of the Schrödinger equation for a spherical potential well. Assuming only the s-wave solution was important, Tersoff and Hamann were led to a simple solution for the tunneling current. Under a low bias the s-wave model shows the

tunneling current to be proportional to the Fermi level local density of states at the center of curvature of the probe r_o (equation 17).

$$I \propto \sum_{E_\mu} |\psi_\mu(r_o)|^2 \tag{17}$$

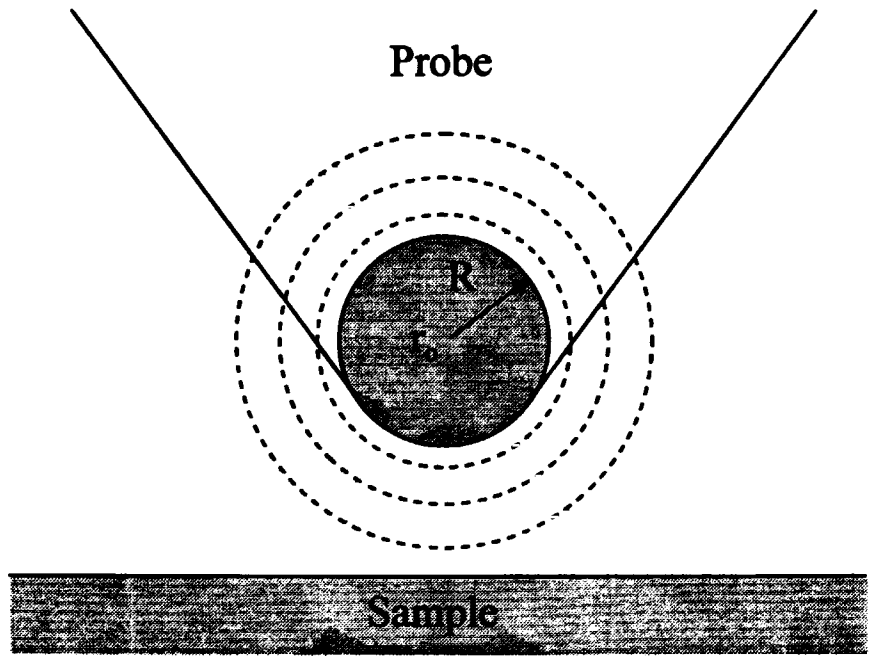

Figure 4. S-wave Probe Model

The s-wave probe model removes the probe interactions from the analysis in a way similar to the point source current model described earlier. Thus, the s-wave model reflects properties of the surface only.

CHAPTER III

DESIGN AND CONSTRUCTION

The first scanning tunneling microscopes operated in ultra high vacuum, were equipped with sophisticated vibration isolation systems, and had minimal computer control. Early experimental work in controlled vacuum tunneling provided some of the groundwork for the first STM built by Binnig and Rohrer. Their first STM was a complicated design that operated in ultra high vacuum and used a primitive liquid helium suspension system for vibration isolation. Analog electronics generated the scanning waveforms and storage oscilloscopes recorded the topographic information. Since then, several designs using a combination of computer instrumentation and analog electronics have been tried but only a few designs have proven successful due to the constraints of STM operation.

Scanning a metal probe over a surface while maintaining a separation of a few angstroms requires very strict design parameters. Mechanical and acoustical vibration, electrical noise, and thermal drift are major impediments to the operation of an STM. For atomic resolution, the probe-sample separation, usually within 10 Å, must be controllable to less than .5 Å. The lateral resolution of the tunneling probe motion must be less than 1 Å. Creating this level of mechanical resolution in the lateral and vertical directions requires a system immune to vibration and thermal drift. The tunneling current measured by the STM is also exceedingly small. Generally, this current varies from several

picoamps to a few nanoamps. Measuring currents at this level requires amplifiers with very high gain and noise immunity.

Advances in computer technology, data acquisition, and digital control systems enable the modern STM to be completely computer controlled. Computer control creates certain advantages as well as additional design constraints. The analog to digital (A/D) converters and the digital to analog (D/A) converters used in the computer control system must have high resolution and sufficient bandwidth to allow for reasonable scan acquisition times.

Even with the rigorous design constraints, scanning tunneling microscopes now routinely operate in a variety of conditions from cryogenic temperatures to 100°C and from ultra high vacuum to liquid environments. The STM designed here operates under computer control in an air environment. Figure 5 shows a block diagram of the system.

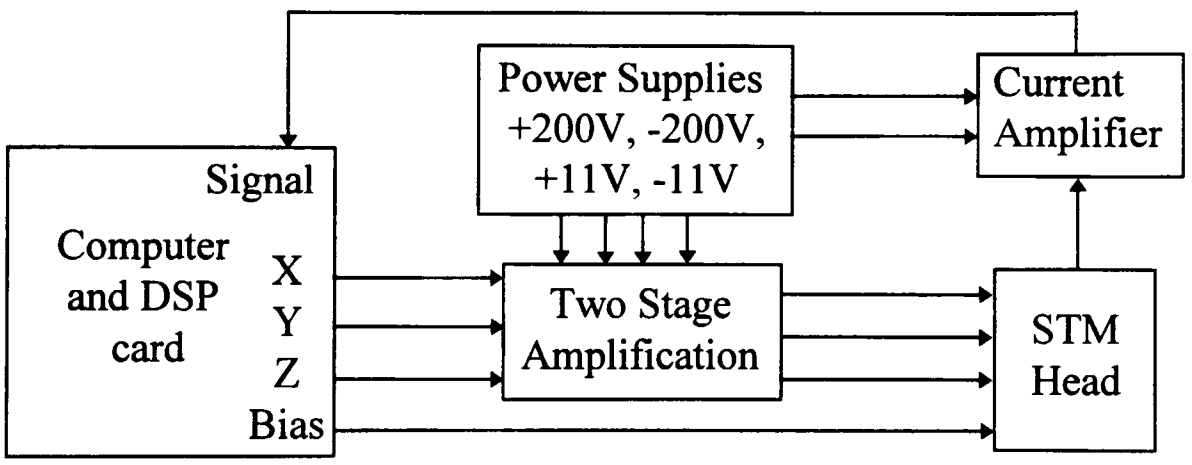

Figure 5. Block Diagram

An IBM compatible computer with a digital signal processor (DSP) interface card generates the waveforms necessary for scanning. To drive the piezoelectric transducers in the STM head, a two-stage amplification system provides a gain of approximately 10.

A current amplifier reads the tunneling current from the STM head and then the DSP card digitizes this information. Three power supplies provide DC power for the piezoelectric amplifiers and the current amplifier.

Piezoelectric Transducers

Piezoelectric transducers are central to the operation of the STM. These transducers provide the finely controlled motion necessary for the demands of STM operation. No other motion control system (e.g., stepper motors) could operate with the precision of piezoelectric actuators.

Pierre Curie and his brother Jacques Curie discovered the piezoelectric effect in 1880. They discovered placing tension on a quartz plate sandwiched between two electrodes produces an electrical charge. Not long after this discovery, Lippman predicted the inverse piezoelectric effect and again the Curie brothers experimentally investigated this phenomenon. In this experiment they used a light-weight lever arm to magnify the displacement produced by applying a potential difference to a long piece of quartz sandwiched between two electrodes. The displacements produced by the inverse piezoelectric effect are very small. Thus, piezoelectric transducers are ideal positioners for scanning tunneling microscopes.[11]

Lead zirconate titanate (PZT) ceramics are the material used in the piezoelectric transducers of an STM. These materials change shape under an applied electric field. Figure 6 shows the behavior of a block of piezoelectric material under an applied electric field. By convention, the poling axis is defined to point from positive to negative. A

piezoelectric material expands along the poling axis when a voltage is applied with the same polarity as the poling axis (V = +).

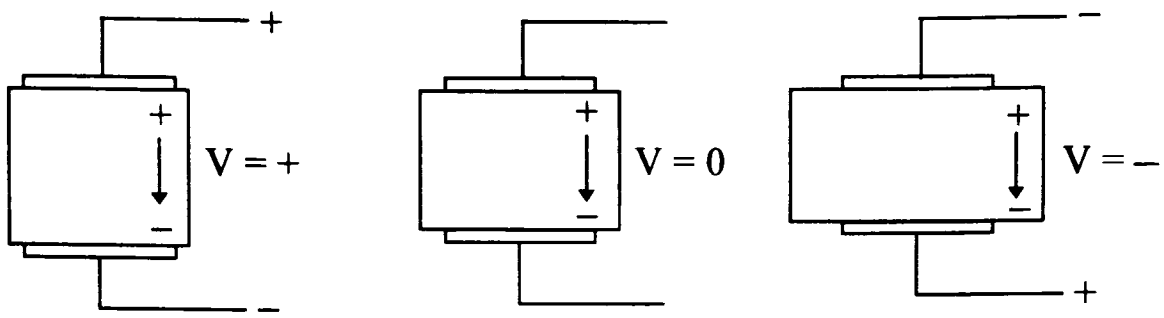

Figure 6. Piezoelectric Behavior

In the direction perpendicular to the poling axis, the material contracts. An applied field opposite to the poling axis (V = –) contracts the material parallel to the poling axis and expands the material perpendicular to the poling axis.[12]

The mechanism producing these displacements in PZT results from the ferroelectric nature of $PbZrO_3$ and $PbTiO_3$. In solid solution, these materials exhibit a permanent electric dipole even in the absence of an electric field. A ceramic solution of the two materials produces an isotropic material due to the random arrangement of the electric dipoles. Permanent polarization is produced by a poling process similar to that of making a permanent magnet from a hard ferromagnetic material. After a PZT is poled it can be used. Since piezoelectric ceramics are not single crystal materials, the anisotropic electric polarization produced by poling is not as stable or reproducible as the piezoelectric effect in single crystal materials such as quartz. Aging, hysteresis, depoling, and temperature sensitivity can change the electric polarization affecting PZT

performance. Most PZT materials can be repoled by applying a suitable voltage at room temperature.[13]

The first scanning tunneling microscope used a tripod scanner arrangement similar to that in Figure 7. Three rectangular arms of piezoelectric material produced the

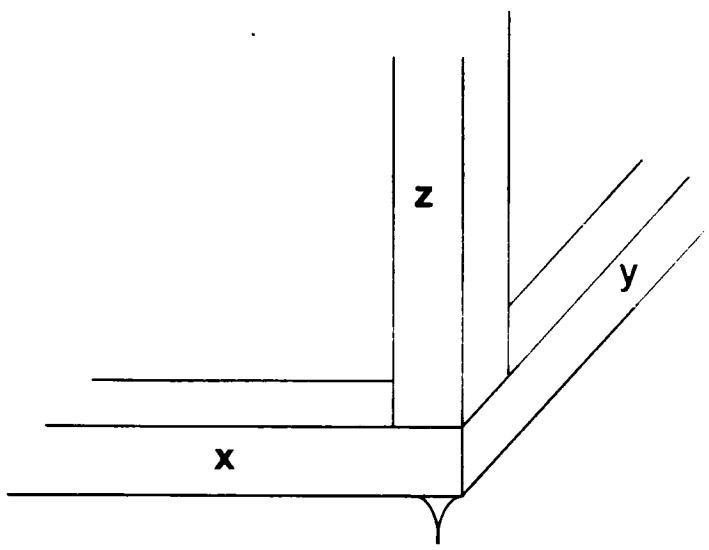

Figure 7. Tripod Piezoelectric Scanner

three orthogonal motions necessary for the STM. The length of the piezoelectric arm changes by ΔL equal to

$$\Delta L = \frac{d_{31} V L}{h} \tag{18}$$

when a voltage V is applied. In equation 18, h is the thickness of the material between the electrodes, L is the length of the rectangular piezoelectric arm, and d_{31} is the piezoelectric coefficient. This coefficient is defined as the ratio of the strain coefficient to the applied electric field (equation 19).

$$d_{31} = \frac{S_1}{E_3} \tag{19}$$

The standard convention labels the directions x, y, and z as 1, 2, and 3. Thus, d_{31} is the ratio of the strain in the x-direction to the electric field applied in the z-direction.

The mechanical design of the scanning tunneling microscope is directly related to the piezoelectric arrangement used to produce scanning motion. The STM must be insensitive to ambient vibrations and thermally stable as possible. These design constraints made the tripod scanner arrangement difficult to use for several reasons. First, the tripod arrangement was difficult to construct. Second, the physical dimensions of the tripod arrangement were large with low resonance frequencies that made the scanner susceptible to ambient vibration. Finally, obtaining calibrated motion in each direction was difficult due to variations in the piezoelectric material of each arm.

To solve some of the problems inherent in the tripod scanner design, Binnig and Smith developed the piezoelectric tube scanner (Figure 8).[14] Piezoelectric tube scanners generally have the tunneling probe mounted in a concentric fashion to one end of the tube. Bending the tube produces the scanning motion (x and y), and changing the tube's

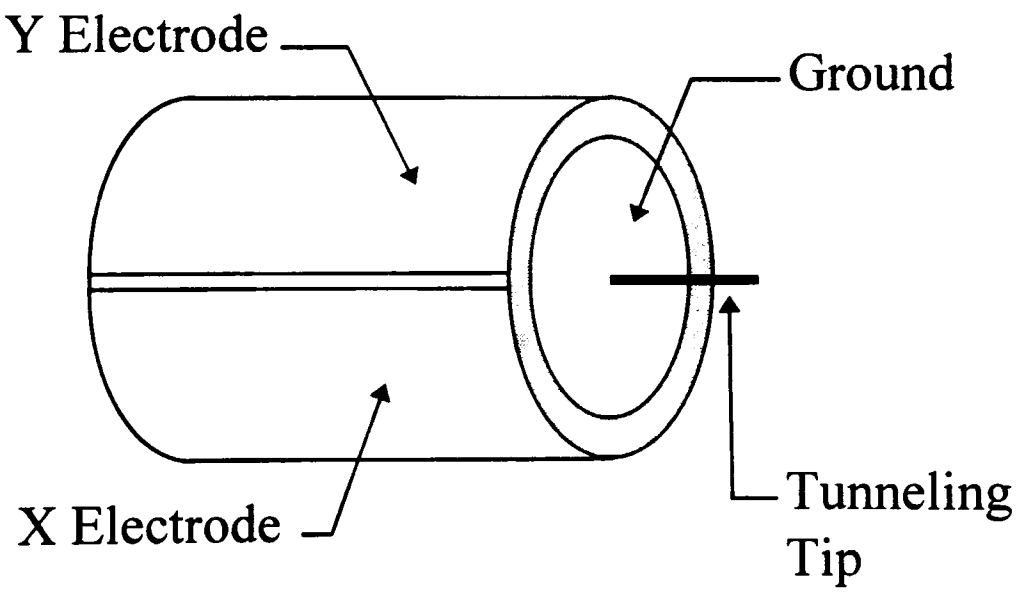

Figure 8. Piezoelectric Tube Scanner

length creates the z motion for the scanner. The tube scanner has several advantages over the tripod scanner. Being one piece of piezoelectric material, the tube scanner is more rigid. Calibrating the deflection in each direction is easier since only one piezoelectric constant must be determined. Most importantly, the piezoelectric tube arrangement allows for the construction of very small scanning tunneling microscopes with high resonance frequencies.

The piezoelectric tubes used for scanning tunneling microscopes are poled radially usually with the outer electrode positive. With this arrangement, applying a negative voltage to all four quadrants of the tube while grounding the inner electrode expands the length of the tube by ΔL given by equation 18.

To create a horizontal deflection in the end of the tube, a voltage is applied to one of the quadrants while the other quadrants are grounded (Figure 9). This voltage changes the length of the corresponding quadrant of the tube creating a horizontal deflection in the end of the tube. Equation 20 determines the amount of deflection.

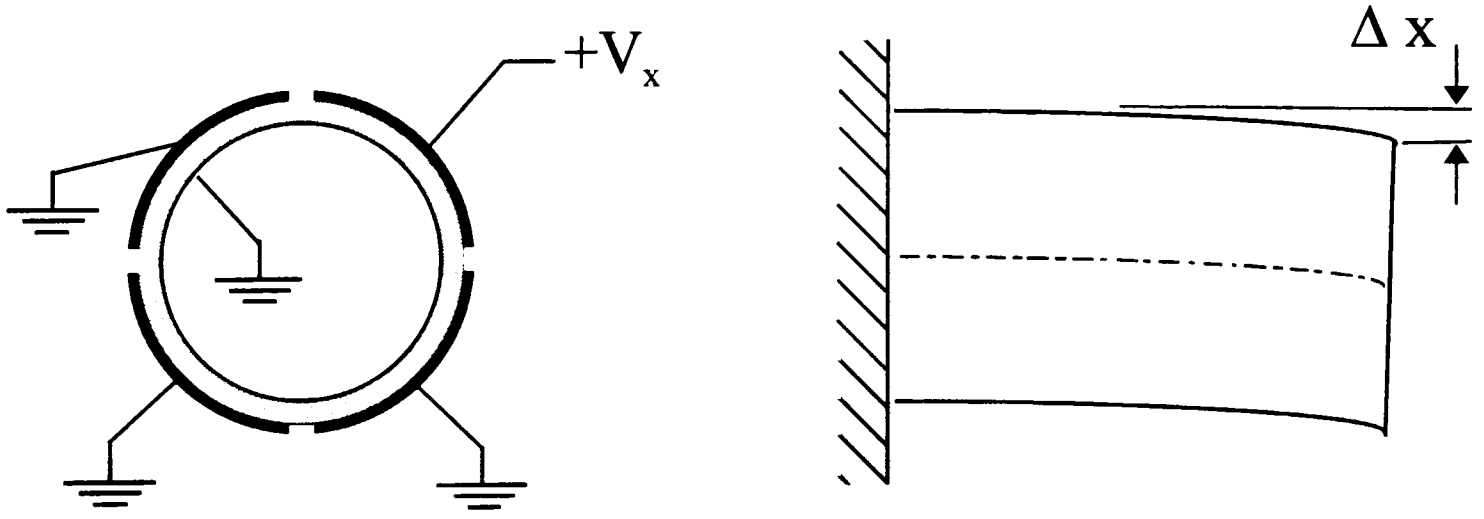

Figure 9. Horizontal Tube Deflection

$$\Delta x = \frac{\sqrt{2} d_{31} V L^2}{\pi D h} \tag{20}$$

V is the applied voltage, D is the diameter of the tube, L is the tube length, and h is the wall thickness of the tube. The sensitivity of a piezoelectric tube may be found by dividing both sides of equation 20 by V. Equation 20 also depends on the piezoelectric coefficient d_{31}, which is usually expressed in Å/V. Typical values for d_{31} range from -1.2 Å/V to -3 Å/V depending on the type of piezoelectric material.[15]

Applying voltages to only two of the four outer electrodes drives the piezoelectric tube in what is called the unipolar mode. The scan range, as well as the sensitivity of the piezoelectric tube, can be doubled in each direction (x and y) by operating the piezoelectric tubes in what is known as the bipolar mode. In this mode of operation, all four electrodes on the outside of the tube are used. A positive voltage is applied to one electrode and a negative voltage of the same magnitude is applied to the opposite electrode (Figure 10).

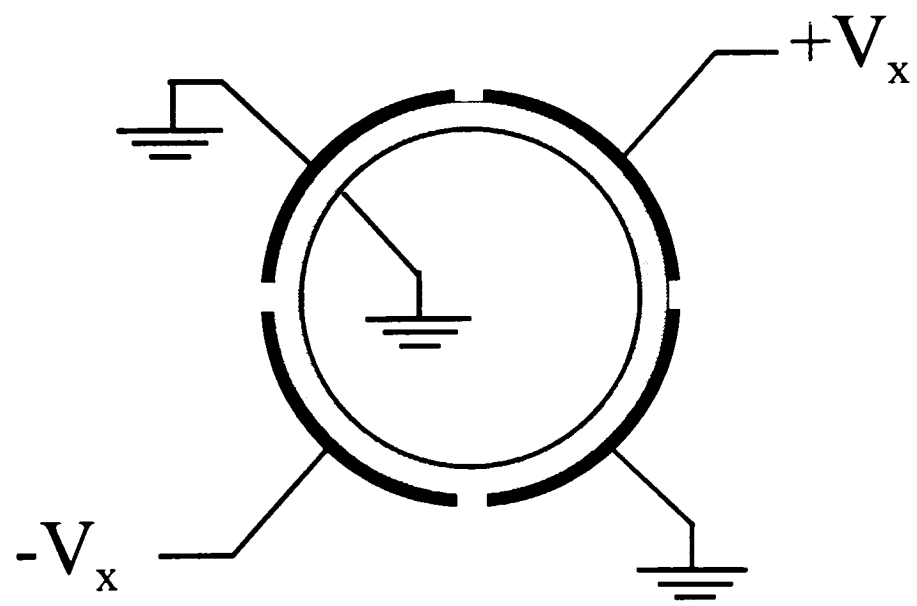

Figure 10. Unipolar Mode

In the bipolar mode of operation, the applied voltage expands one side of the tube and contracts the other side of the tube. Thus, the end of the tube is deflected twice as much as the deflection produced in the unipolar mode.

For the scanning tunneling microscope constructed here, the piezoelectric scanning tube is driven in the bipolar mode. The scanning tube has a diameter of 0.26 inches, a wall thickness of 0.025 inches and a length of one inch. The piezoelectric material of this tube has a d_{31} value of approximately -1.75 Å/V. Thus, the calculated sensitivity of the scanning piezoelectric tube is approximately 242.4 Å/V. The piezoelectric tube used to produce the z motion in this STM has a diameter of 0.48 inches, a wall thickness of 0.040 inches and a length of 1 inch giving the tube a calculated sensitivity of 43.4 Å/V.

The calculated value for the piezoelectric tube sensitivity may not correspond to the actual tube sensitivity for several reasons. For a given type of piezoelectric material, the piezoelectric coefficients are nominal values and vary for individual piezoelectric tubes. Furthermore, the piezoelectric coefficients may decrease if the material is handled improperly. Temperatures above the Curie point (>300 Celsius) and excessive electric fields, greater than 6 kV/cm, applied opposite the poling direction may depole the material. As mentioned previously, since PZT materials are not single crystal, relaxation occurs in the material which also lowers the piezoelectric coefficients. This relaxation is logarithmic in nature and is measured in percent decrease per decade of time. Typical values for this relaxation vary from 0.5% to 6% per decade of time.

Determining the actual values of the piezoelectric coefficients can be done using a variety of methods. Scanning a material with a known lattice size, such as highly oriented pyrolytic graphite (HOPG) can determine the d_{31} coefficient for the scanning tube. Other methods for calibrating piezoelectric constants include using an interferometer, a capacitive displacement sensor, or the double piezoelectric response[16] of the piezoelectric tube. Even after determining the d_{31} constant for a given piezoelectric tube, determining the actual displacement for a given voltage may still be difficult. Many piezoelectric materials suffer from hysteresis and creep effects. Furthermore, at high voltages the piezoelectric tubes do not respond linearly. Thus, at large deflection the actual displacement is difficult to determine.

Tunneling Probe

The condition of the tunneling probe is critical for obtaining atomic resolution. The first STM probe used a tungsten rod 1mm in diameter which was mechanically ground at an angle to produce a sharp probe.[17] Since then, many superior techniques have been developed for manufacturing probes for scanning tunneling microscopes. The most common method utilizes electrochemical etching. Etching the probe with a solution of potassium hydroxide (KOH) or sodium hydroxide (NaOH), produces probes with the properties important for scanning tunneling microscopy. The tunneling probes need an extremely small radius of curvature at the tip. Ideally, the probe needs atomic or near atomic sharpness. Also, the probes need to be short and rigid to prevent vibrations.

Electrochemical etching produces very sharp probes. With this technique tungsten probes with radii of curvature of less than one micron can be produced.

The etching process also forms an oxide coating on the surface of the probe. This oxide prevents tunneling current from flowing, causing the probe to crash into the sample. The oxide must be removed prior to using the probe. Sophisticated methods, such as ion milling, have been developed to accomplish oxide removal; but most of these techniques only work in a vacuum. A simple solution to this problem is to gently crash the probe into the sample so that the oxide breaks, allowing current to flow.

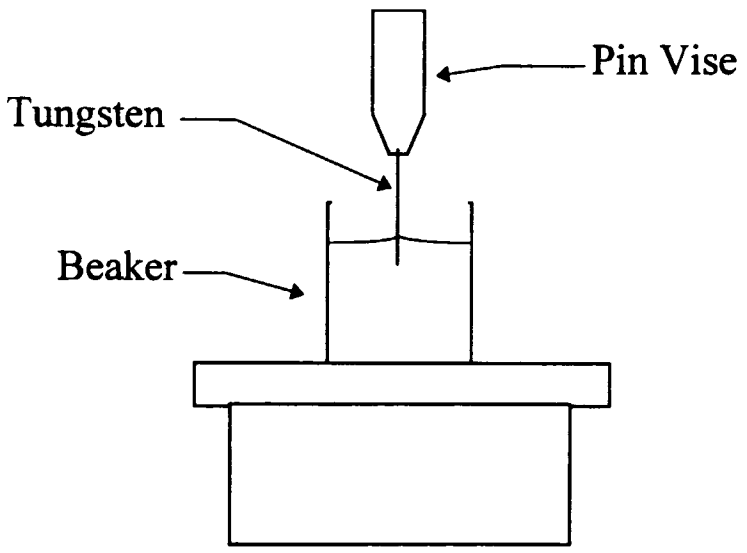

Figure 11. Probe Preparation

Electrochemical etching of the tungsten rods is a simple procedure.[18] The first step is preparing the tungsten rod. The amount of etching current is proportional to the area of tungsten exposed to the solution. To minimize the etching current, the end of the rod is coated with shrink wrap. Maintaining a low etching current is essential. Higher current produces more bubbles at the etching surface. These bubbles make the etching uneven and can cause the lower portion of the tungsten rod to break off prematurely.

After coating the end of the tungsten rod, it is lowered into a 1-2 M solution of NaOH or KOH in a 50 mL beaker until approximately 50 to 80 mA of current flows. At this current level a meniscus forms around the rod just above the heat shrink wrap. A variac provides an AC voltage of approximately 6 volts. When the etching is complete, the lower portion of the rod falls off, breaking the etching circuit. The usable probe is just above the surface of the solution. This method of preparation automatically shuts off the etching current as soon as the lower portion of the rod breaks away.

Producing a sharp probe depends on several factors, the most important being the time of etching after the lower portion of the rod has fallen away. The procedure selectively etches away a small portion of the tungsten rod. Eventually the rod becomes so thin that the lower portion falls away. The etching current must be shut off as quickly as possible after the rod falls away to produce the sharpest probes. Several methods employing electronic circuits can automatically shut off the etching current; but, as mentioned previously, by etching the rod at the meniscus of the solution-air interface, the etching current is automatically shut off when the rod falls away.

Several tunneling probes have been produced with the aforementioned method. In some cases, the rod was positioned too low in the solution, resulting in the etching of the probe after the lower portion of the rod had fallen away. Under a scanning electron microscope, many of the probes produced appear to have a radius of curvature of less than 1 micron.

Mechanical Design

Mechanical Design Constraints

The mechanical structure of the scanning tunneling microscope requires a high degree of vibration isolation and thermal stability. Generally, for scanning tunneling microscopes the probe is within a few angstroms of the sample surface. Any vibration of the probe with respect to the sample is of great concern. To prevent vibration of this type both systems must be strongly coupled together. Furthermore, the entire assembly should be as small and mechanically rigid as possible. A small, mechanically rigid system is less susceptible to ambient vibration due to the higher resonant frequencies of the system. Thermal stability is also of concern. Construction materials need similar thermal properties as thermal drift between the probe and sample must be minimized. The design used for this STM uses a piezoelectric tube scanner and is based on a design by Lyding and coworkers.[19] This design utilizes two piezoelectric tubes to provide for coarse probe-sample positioning and thermal compensation.

Scanner Design

Numerous STM designs employing piezoelectric tubes have been developed.[20-23] The common feature of all of these designs is the small size of the microscope. Although STMs designed with piezoelectric tube scanners have an excellent immunity to vibration because of their small size, coarse sample positioning can be a problem. The two-tube design solves the coarse positioning problem for the probe-sample positioning; but x and y coarse positioning is difficult to implement in this design.

This STM uses two piezoelectric tubes. One tube is of a smaller diameter than the other and is mounted concentrically inside the other tube to an aluminum collar (Figure 12). The outer tube maintains the probe-sample distance and the inner tube is used for the scanning motion. The inner tube has the tunneling probe attached in a coaxial fashion. This setup shields the tunneling probe from any external interference since the inside of the scanning tube is grounded. The outer piezoelectric tube has another aluminum collar mounted to its other end. This collar holds the sample tube containing the brass translation rods.

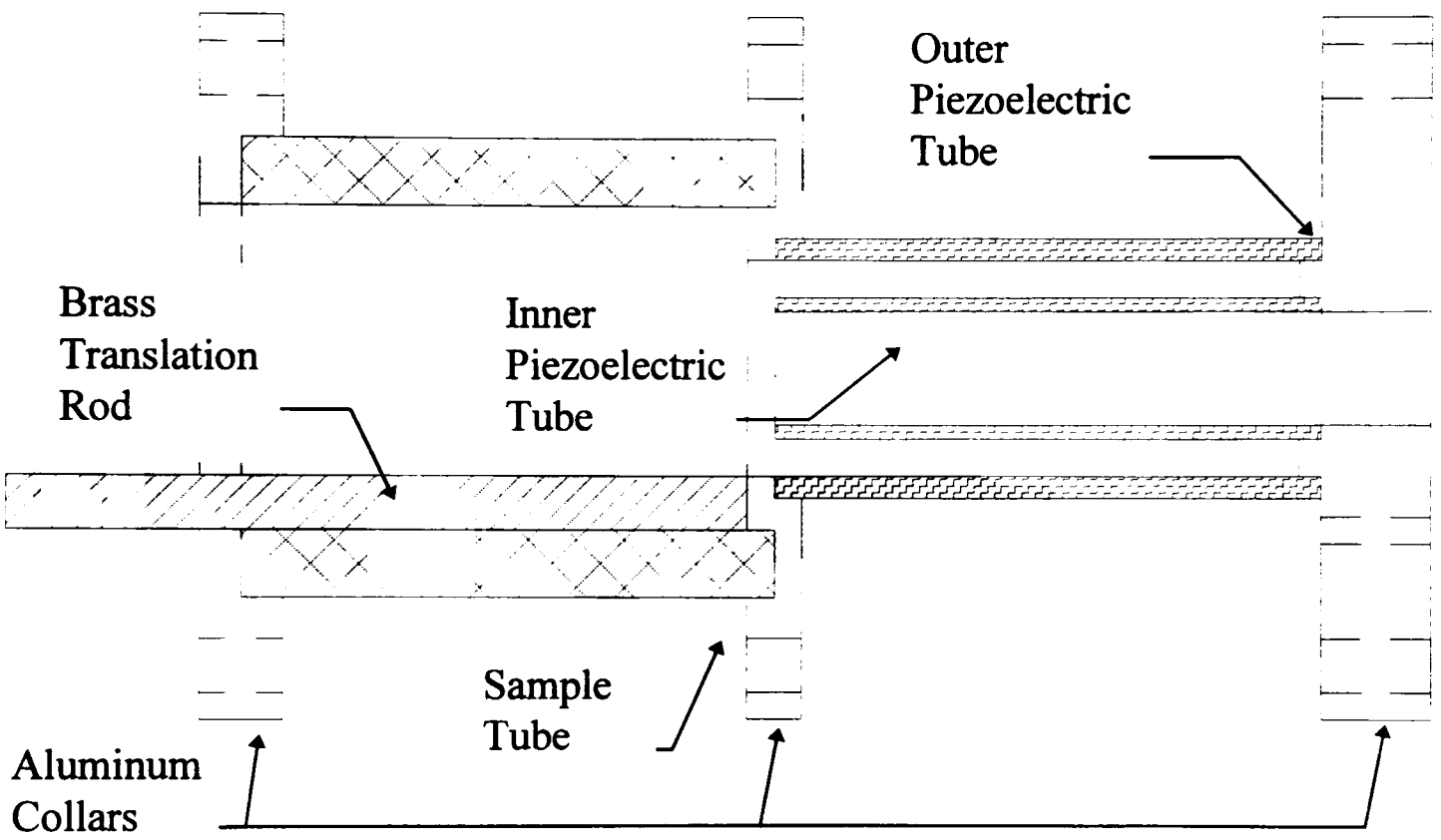

Figure 12. Two-Tube Design

An additional feature of this design is the method of thermal compensation. The outer tube expands along with the inner tube as the temperature of the microscope changes. Some thermal expansion of the sample tube can still produce thermal drift. But

by fabricating the sample tube and sample holder from a material with a very low thermal expansion coefficient, thermal drift can be reduced and the microscope can be operated from liquid helium temperatures to up to 100 °C.

Coarse Sample Positioning

Coarse sample positioning presents a challenging design problem in the STM. A variety of methods have been developed for coarse positioning of the sample. Stepper motors, lever and spring motion demagnifiers, and inertial sliding techniques have been tried. For the x and y directions, coarse positioning systems allow large areas of the sample to be imaged. For the z-direction, the coarse positioning system must be able to provide a fine enough stepping motion to bring the tunneling probe and sample close enough for tunneling to take place. These systems must also be able to translate the sample over macroscopic distances. Many of the coarse sample positioning methods create unacceptable levels of vibration or cannot provide a fine enough motion without crashing the probe into the sample. For example, stepper motors work well for producing controlled motion adjustments; but the heat produced by the motor may create problems with thermal drift. More importantly, stepper motors may create unacceptable vibrations, causing the probe to crash into the sample. Coupling the additional mass of a stepper motor to the STM lowers the natural resonance frequency of the system, making it susceptible to ambient vibration. Lever motion demagnifiers work well in that very fine adjustments can be made, producing step sizes small enough to avoid crashing the probe

into the sample. However, these methods are not automated unless a stepper motor is employed.

For coarse positioning, several methods that are based on the inertial sliding method have been developed. The inertial sliding method, also known as the "stick-slip" method, works because the kinetic coefficient of friction (μ_k) between two surfaces is less than the static coefficient of friction (μ_s). First described by D.W. Pohl, a saw tooth voltage waveform is used to produce motion of a sample stage.[24] Figure 13 shows the general inertial slider setup.

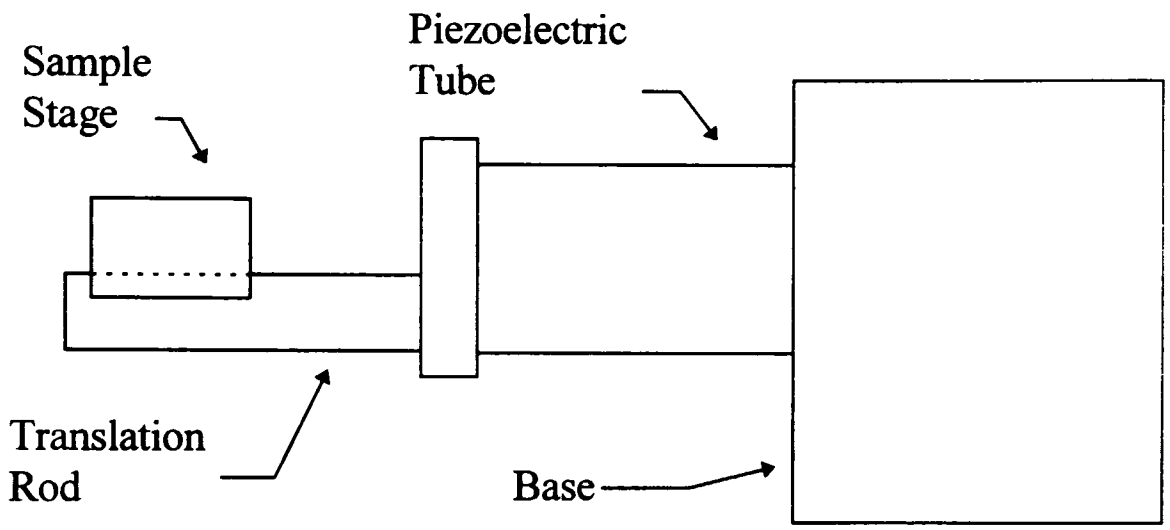

Figure 13. Inertial Slider Setup

As the voltage ramps up, the length of the piezoelectric tube contracts. The position of the translation rod follows the voltage applied to the piezoelectric tube. For a saw tooth voltage, the translation rod slowly moves inward as the piezoelectric tube contracts. The static frictional force ($\mu_s F_N$) between the sample stage and the translation rod causes the two pieces to move inward as the piezoelectric tube contracts. At the peak of the waveform, the abrupt voltage drop rapidly expands the piezoelectric tube,

producing a large acceleration in the translation rod. The large acceleration of the translation rod produced by this voltage change causes the translation rod to slip underneath the sample stage. The inertia of the sample stage keeps it in place. For a given sample stage with mass m and a static coefficient of friction, μ_s, the acceleration of the rod must satisfy equation 21 for sliding to occur.

$$a_s > \frac{\mu_s F_N}{m} \tag{21}$$

Ideally, the acceleration of the translation rod is roughly proportional to the second derivative of the coarse positioning waveform. Figure 14 shows a saw tooth waveform used for moving the sample towards the tunneling probe. The DSP card in the computer produces the upper waveform in Figure 14. The translation rod displacement follows a waveform similar to the lower waveform in Figure 14 due to the finite response of the piezoelectric tube. A qualitative estimate of the translation rod acceleration is determined from the change in the slope of the waveform.

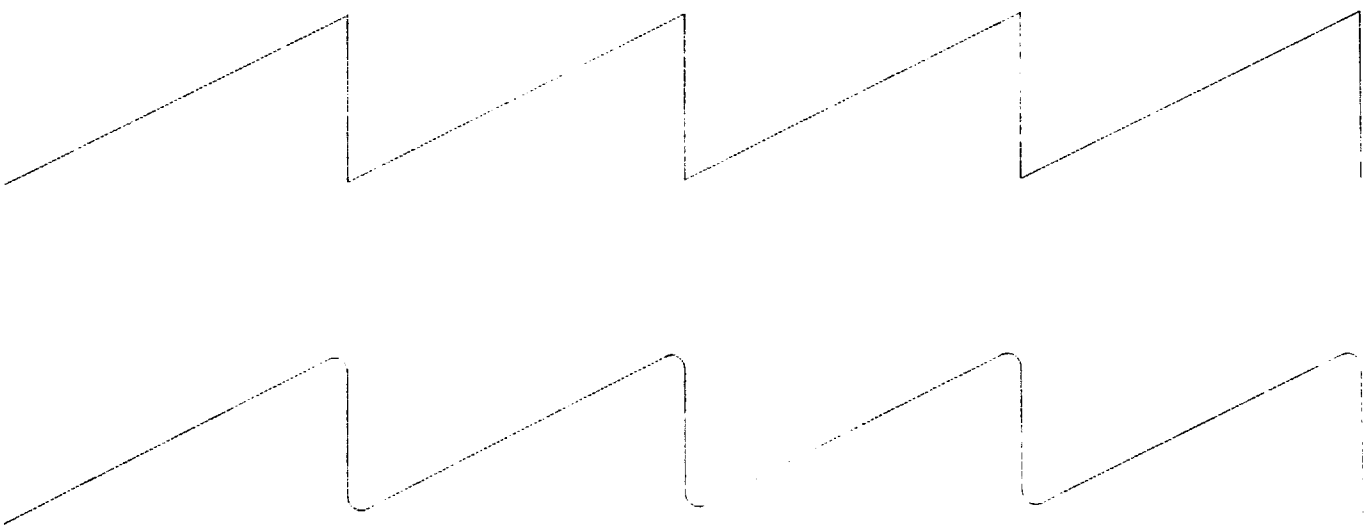

Figure 14. Saw Tooth Wave

Generally, this acceleration easily exceeds the value necessary to overcome the frictional force of the sample stage. The change in slope from positive to negative produces acceleration in the rod that moves the sample stage towards the tunneling probe. The next acceleration results from the slope changing from negative to positive. This acceleration moves the sample stage away form the tunneling probe. Thus, the saw tooth waveform does not produce the most reliable motion of the sample stage because of these two opposing accelerations. A waveform producing acceleration only in one direction is superior to the saw tooth wave. The digital signal processor in the computer can produce any analytic waveform. A waveform such as that in Figure 15 has only one sharp peak. This wave produces acceleration in only one direction and moves the sample stage towards the tunneling probe. To move the sample away from the probe, the polarity of the wave is inverted. The voltage of this wave has a cubic dependence on time. Other types of waves, such a cycloid, have also produced acceptable results.[25]

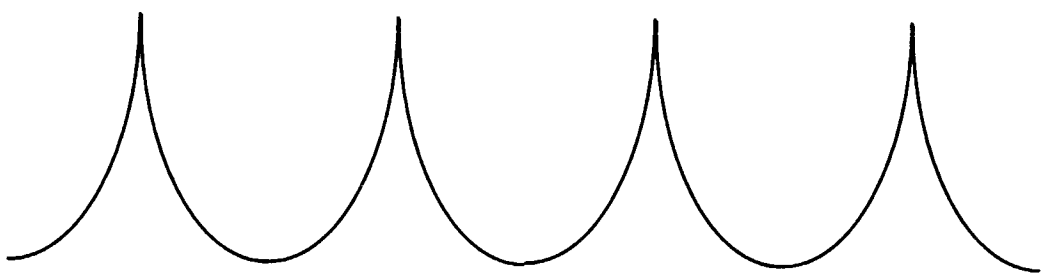

Figure 15. Coarse Approach Waveform

The waveform in Figure 15 produces sample stage motion towards or away from the tunneling probe in steps of varying size depending on the amplitude and frequency of the wave. The amplitude and frequency of the wave are set by the user. The upper limit of the frequency depends on the resolution of the wave and the maximum conversion

speed of the digital to analog converter. A threshold frequency and amplitude exist for which the wave does not produce sufficient acceleration to move the sample stage.

Vibration Isolation

The first scanning tunneling microscopes required complicated systems for vibration isolation. The tube scanner design requires minimal vibration isolation in comparison. In fact, a single stage spring and dampener system is sufficient. For the STM described in this paper, a large aluminum block and a bicycle inner tube make up the vibration isolation stage. The block is approximately 12"x12"x4". A small bicycle inner tube is glued to the bottom of the block. This configuration can be analyzed as a vibrating system with one degree of freedom. The bicycle inner tube acts as the spring and the dampener (Figure 16).

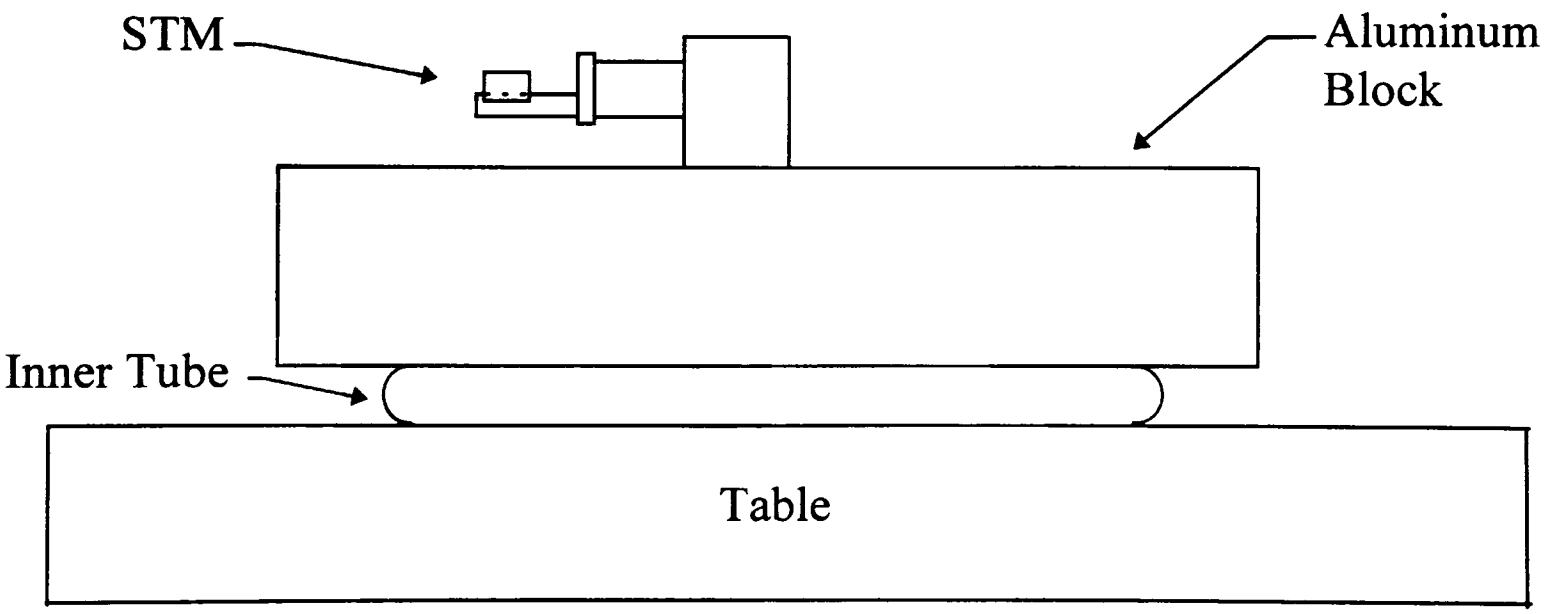

Figure 16. Vibration Isolation System

Vibrations coupled acoustically to the microscope are of more concern than vibrations coupled through the table or floor. Cooling fans in the computer and the piezoelectric amplifiers produce 60 Hz vibrations. Enclosing the STM head lessens some of the acoustically coupled vibration. Moving the fans as far away as possible is the only other solution aside from enclosing the microscope in vacuum.

Electrical Design

Analog test equipment generated the scanning waveforms, and analog feedback and control circuits provided the necessary control for the first STMs. Computers were used only for recording the tunneling current information. Advances in computer technology and data acquisition systems allow for modern scanning tunneling microscopes to operate under complete computer control. The STM designed here uses a computer for all functions involved with the microscope.

Electrical Design Constraints

Three major electrical systems comprise the instrumentation for the STM—the current to voltage (transimpedance) amplifier, the piezoelectric driver amplifiers, and the digital signal processor data acquisition card. Each component must be as noise free as possible. Each component must also have sufficient bandwidth to allow for reasonable scan times.

Electrical Noise

Electrical noise often sets limits to the performance of an instrument. For the scanning tunneling microscope designed here, noise in the transimpedance amplifier and in the piezoelectric drive amplifiers are of greatest concern.

Shot noise and Johnson noise are generally the limits to reducing noise in electronic systems. Johnson noise, also known as thermal noise, results from the thermal motion of electrons. The power of the noise, given by equation 22, is proportional to the frequency bandwidth, Δf, and the temperature T.

$$P = 4k_b T\Delta f \tag{22}$$

k_b is Boltzmann's constant. The root mean square (rms) Johnson current noise through a resistor R is[26]

$$I = \sqrt{\frac{4k_b T\Delta f}{R}}. \tag{23}$$

At room temperature, with a 66 MΩ resistor and a 3 kHz bandwidth the rms noise is approximately .87 pA. Shot noise results from the discrete nature of the electric charge.

$$I = \sqrt{2qI_{dc}\Delta f} \tag{24}$$

The rms value for the shot noise can be determined from equation 24. In this equation, I_{dc} is the average direct current, q is the electron charge, and Δf is the bandwidth. Unless the bandwidth of the system is very large, or the current being measured is much less than 1 pA, the shot noise can usually be neglected.

Noise in the piezoelectric drive amplifiers translates into unwanted motion of the tunneling probe with respect to the sample. The shot noise and Johnson noise in the

piezoelectric drive amplifiers can safely be ignored. Noise in this system results from interference or from ground loops. The amount of tolerable noise in this amplification system is generally related to the sensitivity of the piezoelectric tubes used in scanning and maintaining the probe-sample separation. For example, if the sensitivity of the scanning piezoelectric tubes is 250 Å/V, then amplifier noise on the order of 5 mV creates more than an angstrom of movement at the tunneling probe. Thus, the noise of the amplifiers must be very low for high sensitivity tubes. A simple solution to this problem would be to have a piezoelectric tube with low sensitivity. But this arrangement reduces the overall scanning range of the microscope for a given drive voltage.

For the transimpedance amplifier, shot noise and Johnson noise must be examined more carefully. Since the bandwidth of the transimpedance amplifier is relatively low, less than 10kHz, the shot noise is much less than a picoamp and can be ignored. The transimpedance amplifier has a 66 MΩ feedback resistor. This resistance with the 3 kHz bandwidth translates to a rms Johnson noise of less than 1 pA. More serious problems concerning the transimpedance amplifier result from capacitive coupling. The high input impedance of the current amplifier makes it very susceptible to capacitive coupling. Proper shielding of the input to this amplifier can reduce capacitive coupling.

Transimpedance Amplifier

The most important circuit in an STM is the current to voltage amplifier used to amplify the tunneling current. The tunneling current ranges from a few 100 pA to 10 nA; thus, a very sensitive current amplifier is necessary to obtain a good signal. The bias

voltage driving this tunneling current is usually 100 mV to a few volts in magnitude. With these values of current and voltage the resistance of the gap between the probe and the sample varies from hundreds of MΩ to a few GΩ. The high resistance of this gap and the low tunneling currents require an amplifier with very high input impedance and a low bias current. The Analog Devices AD549 operational amplifier (opamp) possesses these characteristics. The bias current of the AD549 is on the order of femtoamps and the input impedance is approximately 10^{11} ohms, which is sufficiently high for amplifying the tunneling current.

Proper layout and construction of the transimpedance amplifier is essential to maintaining high current sensitivity, low noise, and sufficient bandwidth. Leakage currents can destroy the high sensitivity of the AD549. To minimize the effects of leakage currents, the AD549 inverting input pin is guarded and both inputs are isolated from the printed circuit board with Teflon. The connection between the opamp and the tunneling probe also deserves special attention. This connection should be as short as possible for several reasons. First, vibration of the connection wire can create piezoelectric effects and friction can create triboelectric charges. Second, a shorter connection also lowers susceptibility to stray fields and parasitic capacitance. The connection to the tunneling probe is via a short piece of coaxial cable that is grounded on one end only. This grounding method reduces the effective input capacitance and thus any noise generated by the "microphone effect."

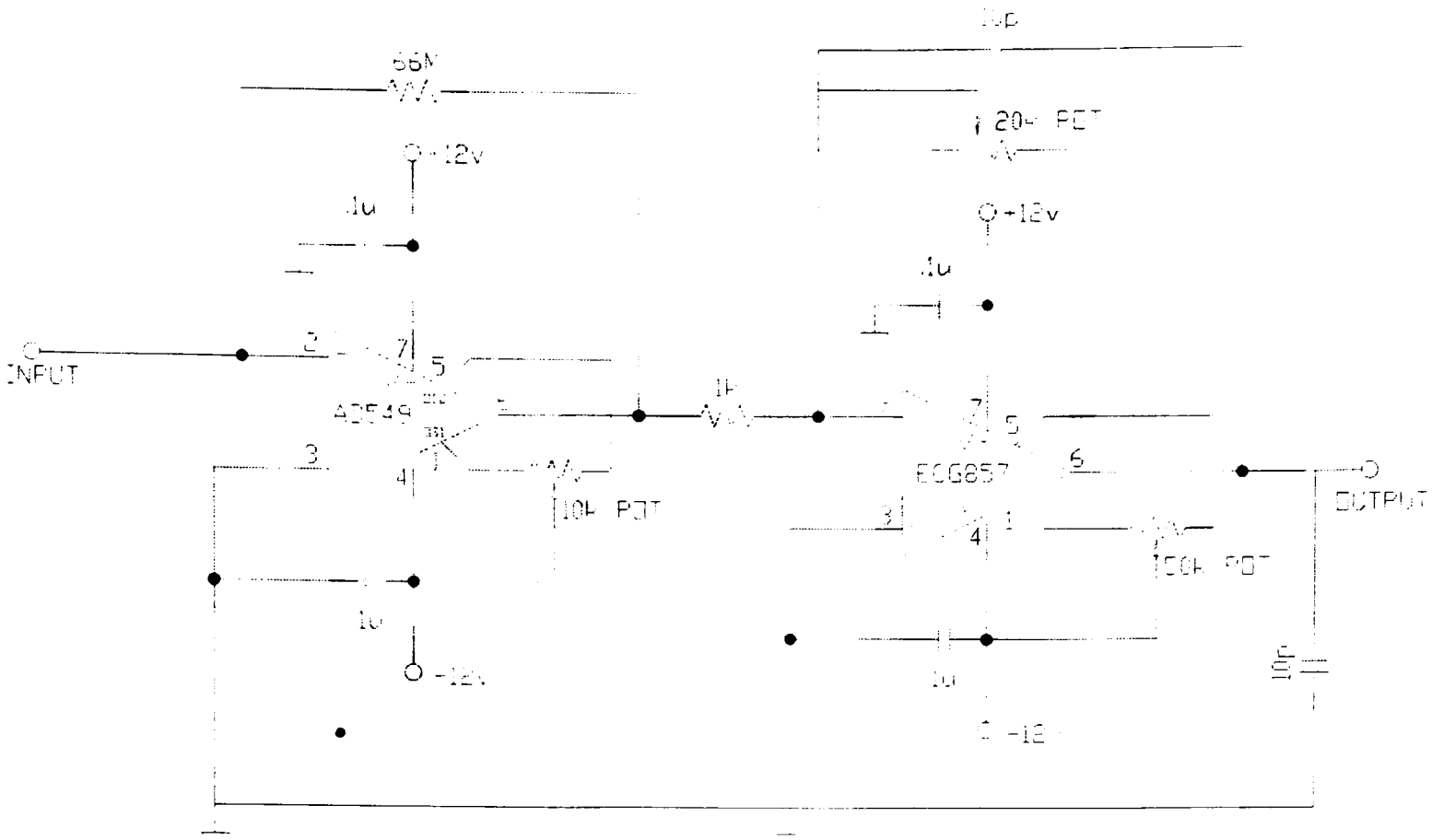

Figure 17. Transimpedance Amplifier

The transimpedance amplifier shown in Figure 17 consists of a two-stage system. The first stage has a gain of approximately 66 million. The second stage adjusts any offset and trims the gain. The output of the second stage has a range of -10 V to 10 V to match the analog to digital converter range on the DSP card. Both circuits are built on printed circuit boards and enclosed in a metal box with BNC connectors.

A low noise metal film resistor made by Victoreen was used for the feedback resistor of the AD549 operational amplifier. The stray capacitance between input pin two and output pin six of the AD549 is less than one picofarad. With the feedback resistance of 66 MΩ, the bandwidth of the amplifier can be estimated from equation 26.

$$f = \frac{1}{2\pi R_f C_f} \leq 5kHz \tag{26}$$

R_f is the feedback resistance and C_f is the stray capacitance between the input and output pins. The bandwidth of the amplifier can be significantly increased using a resistor network or a compensation capacitor.[27] Both of these techniques increase the Johnson noise of the amplifier; but the bandwidth can be increased by over an order of magnitude.

Piezoelectric Amplifiers

Creating a substantial deflection in the piezoelectric tubes requires voltages up to 100 V. Preamplifiers and driver amplifiers create this voltage necessary for scanning the sample surface and maintaining the probe-sample distance. Ideally, these amplifiers must have rms noise less than 1 mV and a bandwidth in excess of 10 kHz.

The amplifier setup consists of a two-stage system. The first stage has five preamplifiers that provide unity gain. +12 V and –12 V power this stage. These amplifiers also have an adjustable dc offset and an adjustable gain for trimming the output signal. Each preamplifier uses a low noise JFET opamp—the Analog Devices OP07—that is mounted on a printed circuit board.

For each scanning direction (x and y), two preamplifiers split the output signal from the computer into an inverted and noninverted signal so that the scanning tube may be driven in bipolar mode (Figure 18). These signals are then amplified by the second stage.

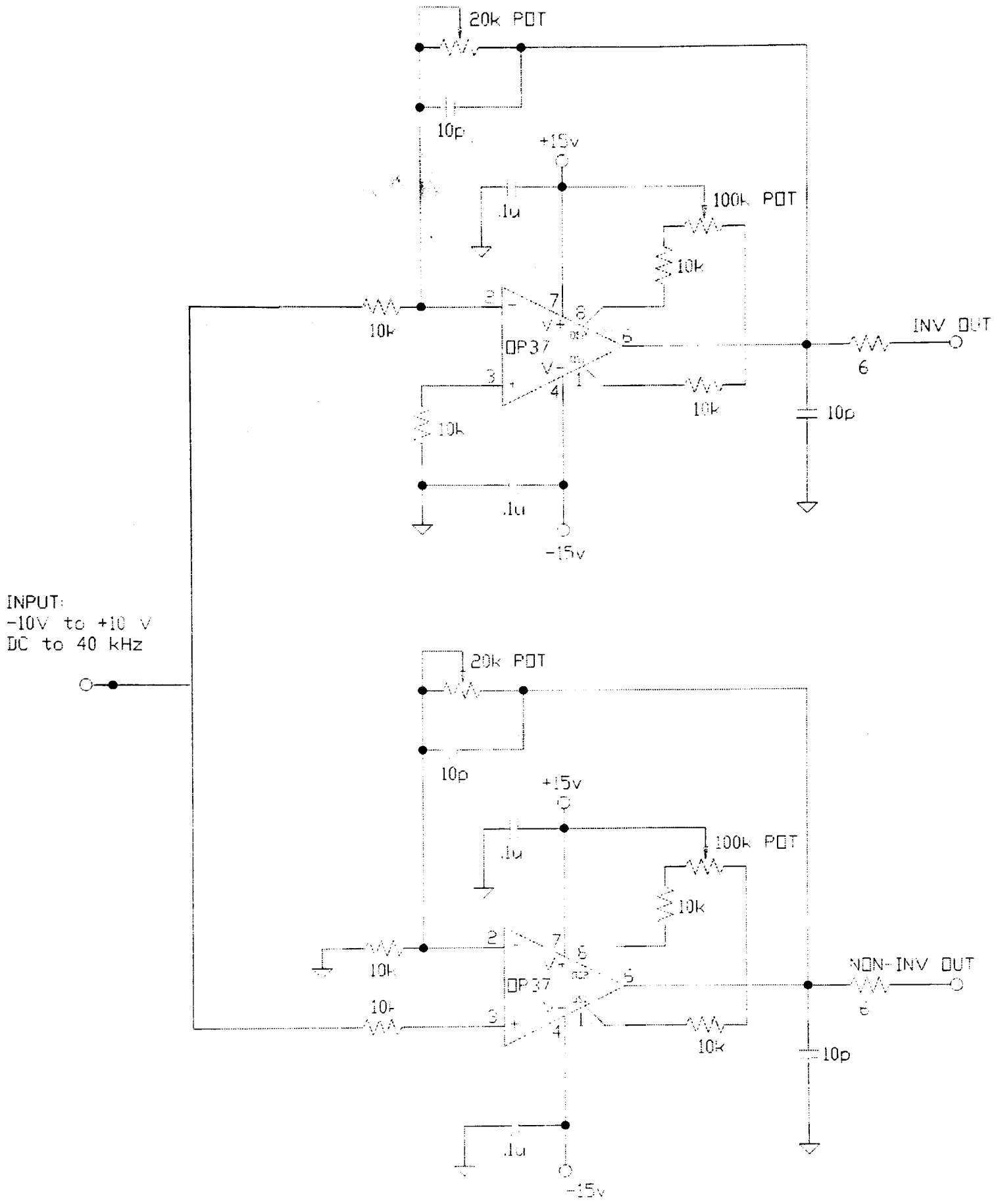

Figure 18. X and Y Preamplifiers

The second stage provides a gain of approximately ten using the PA85 low noise high slew rate opamp. The PA85 opamp, made by Apex Microelectronics, has a very high slew rate (~ 1000 V/μS) and a maximum peak to peak voltage output of 420 volts. Designed for driving piezoelectric transducers, the amplifiers for this STM are based on application notes provided by Apex.[28] Five amplifiers are used—one for each preamplifier. Four of these amplifiers drive the inner scanning piezoelectric tube and the fifth amplifier drives the outer z positioning piezoelectric tube. All of the amplifiers are inverting and identical in design. Figure 19 shows a schematic for of the design.

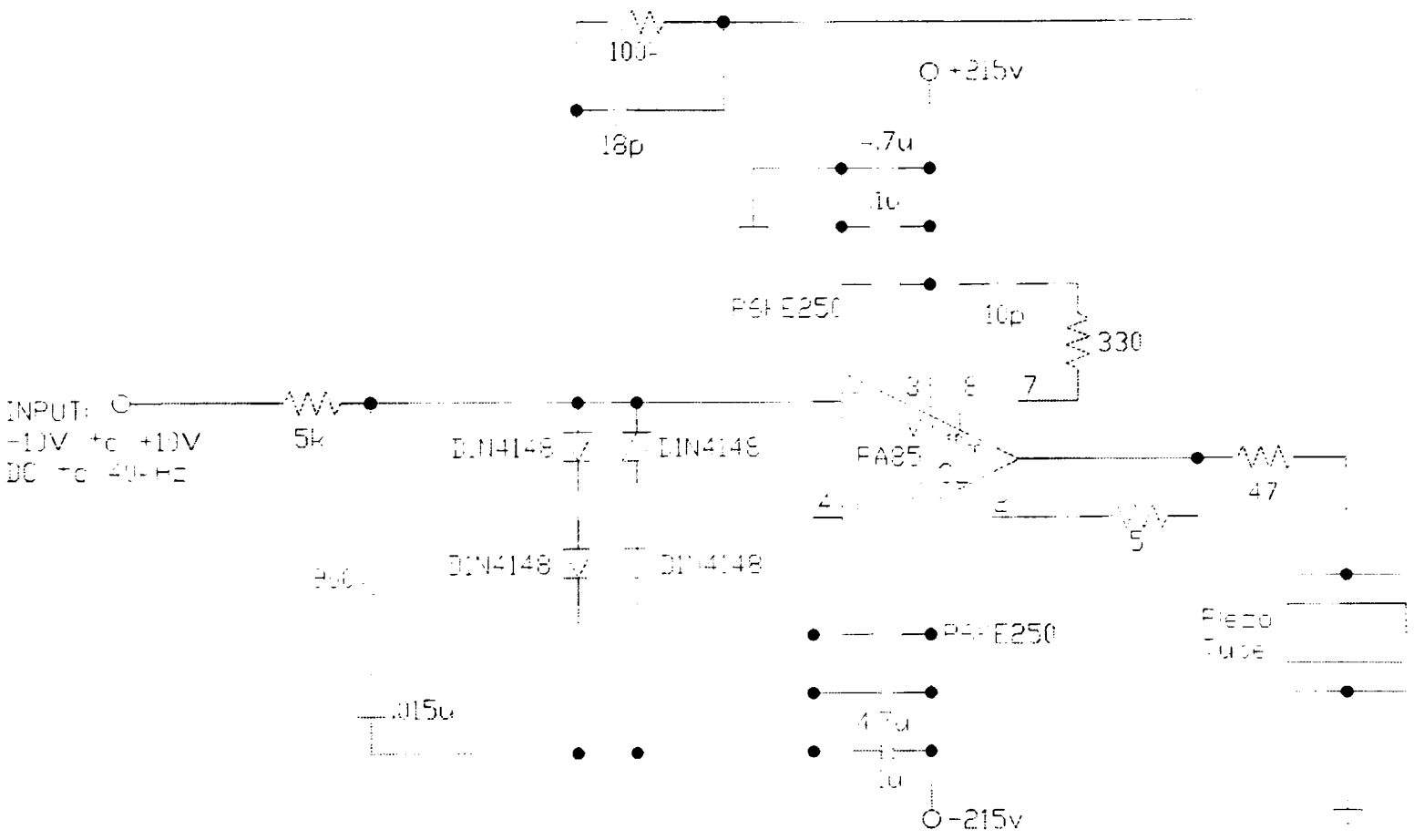

Figure 19. Second-Stage Piezoelectric Amplifier

Due to the voltage and current characteristics of the amplifiers, they must be mounted on heat sinks. The opamps are mounted to the printed circuit boards through an

aluminum plate. Heat sinks are attached to the top side of the opamp on the other side of the plate. Each pin has a short Teflon sleeve around it to prevent electrical contact with the aluminum plate. When the opamps are being operated for extensive periods of time, two fans provide additional cooling. The fans cannot be used when data is being collected due to the acoustic noise generated.

Capacitive loading is a major problem with these amplifiers regarding stability. The inner piezoelectric tube has a capacitance of approximately 15 nF and the outer tube has a capacitance of about 20 nF. The effect of this capacitance can produce instability in the amplifier. An extra resistor mounted at the output of the opamps reduces the effect of this capacitance.

Power Supplies

Three power supplies provide power to the piezoelectric drive amplifiers and the transimpedance amplifier. Two of the power supplies provide the necessary +200 V and –200 V for the second stage of the piezoelectric drive amplifiers. The third power supply provides +12 V and –12 V for the first stage of the piezoelectric drive amplifiers and the transimpedance amplifier.

Computer Control and Software

Computers have played a role in scanning tunneling microscopy since nearly the inception of the field. Usually the computer served the purpose of displaying the topographic information and analog electronics controlled the microscope. Until

recently, high quality computer instrumentation capable of meeting the requirements for scanning tunneling microscopy has been very expensive. Using computer-generated waveforms requires D/A converters with 16-bit resolution. The resolution is required for high sensitivity piezoelectric tubes. For example, a 16-bit converter used over a 20 V range has a resolution of approximately .3 mV/step. After the output is amplified by the piezoelectric drive amplifiers with a gain of ten, the voltage resolution is approximately 3 mV/step. For a scanning piezoelectric tube with a sensitivity of 250 Å/V, the smallest D/A change possible produces a .75 Å change in the position of the tunneling probe. With 12-bit D/A converters this value increases to over 10 Å. For analog signal acquisition, 16-bit A/D converters are necessary for performing advanced techniques such as scanning tunneling spectroscopy.

The computer system containing the data acquisition card provides for the microscope control, data acquisition, and the image display. The computer is an AMD k5 processor running at 100 MHz with the Windows95 operating system. The data acquisition card is the PC32 Supercontroller made by Innovative Integration.

Data Acquisition Card

The PC32 Supercontroller is an industry standard architecture (ISA) data acquisition card (DAC) that creates the scanning raster signals and records the tunneling current amplified by the transimpedance amplifier. This DAC meets the instrumentation requirements for scanning tunneling microscopy for less than 1500 dollars. Other

systems with similar performance characteristics were much more expensive, ranging from 3000 to 7000 dollars.

The DAC has a Texas Instruments TMS320C32 digital signal processor which controls the STM. This 40 MHz DSP is capable of simultaneously creating the scanning waveforms, collecting data, and performing digital feedback and control for the STM. The central processor unit (CPU) in the host computer is also capable of performing all of these tasks; but modern operating systems periodically interrupt the CPU. These interrupts would make implementing a digital feedback and control loop impossible. Thus, all microscope control is handled by the DSP leaving the computer CPU available for manipulating data.

For analog interfacing, the DAC has four A/D converters and four D/A converters with 16-bit resolution. The performance of these converters is comparable to instrumentation grade equipment.[29] Each of these converters has a minimum conversion time of 10 μs which corresponds to a maximum operational frequency of 100 kHz. Two 32-bit internal timers provide a trigger signal for the converters. They can be software or hardware triggered; but using the timer as a trigger source ensures synchronized conversions and provides a uniform sample rate.

The DAC plugs into an ISA slot on the computer motherboard. Two direct memory access (DMA) controllers onboard the DAC are available for transferring data to and from the host computer. Data may also be transferred through dual port random access memory (RAM), which is a 1 kilobyte 32-bit wide block of memory accessible by the host computer and the DSP. Control of the dual port memory is arbitrated though the

use of hardware semaphores. The DSP or the host computer processor can access the semaphores. When a semaphore is accessed, the other processor is unable to use the semaphore until it has been released. This scheme prevents both processors from trying to access the dual port memory simultaneously.

DSP Feedback and Control System

Digital feedback and control systems have some advantages when compared to analog feedback and control systems. The primary advantage of digital control systems is the flexibility of the type of control system. Changing the system from proportional to proportional-integral (PI), or to any variety of control algorithms, only requires reprogramming the DSP. For analog feedback and control, changing the control system usually requires rebuilding hardware.

Proportional-integral-derivative (PID) feedback is a common method of implementing feedback and control. In this system, the control output is the sum of three separate feedback loops. One loop corresponds to the proportional control. Another loop is integral control. The third loop is derivative control. Each feedback loop modifies the difference between the input and a set point value. This difference is the error. For proportional feedback, the control output is equal to the error multiplied by a constant, called the proportional gain. For integral control, a constant, called the integral gain, is multiplied by the integral of the error. Derivative control multiplies the derivative gain constant by the derivative of the error signal. For analog control systems the integral and

the derivative of the error can be determined using opamps. For digital control systems, approximations for the derivative and integral of the error must be used.

Implementing PID feedback in code uses equation 27.[30] In this formula, Z_t is

$$Z_t = Z_{t-1} + E_t(P + I + D) + E_{t-1}(I + D), \tag{27}$$

where E_t is the error value at time t. P, I, and D are proportional, integral, and derivative gain constants. The behavior of the digital feedback and control system depends on the sampling rate of the system. For this reason, ensuring that the sampling is periodic is mandatory. As mentioned previously, triggering the data acquisition with the DAC timers ensures the sampling rate is periodic.

DSP Software

The software for the DSP onboard the DAC card was written in C. A listing of this program is in the Appendix. When loaded into the DSP and executed, the program enters a continuous loop waiting for instructions from the host computer. Upon receiving an instruction, the program executes the function associated with that instruction. The program has functions for coarse positioning, feedback adjustment, feedback parameter testing, and scanning. All functions invoke interrupt service routines (ISR) to perform the required data acquisition or waveform generation. These routines execute at periodic intervals specified by the user. To end the continuous loop the user exits the graphical interface. This action stops the program and resets the DAC.

A PID digital feedback and control loop maintains probe-sample separation distance. The code for this function is interrupt driven using equation 27 for determining

the output signal for the z piezoelectric tube. This function also creates the scanning waveforms for the x and y deflection. At each user-specified timer interval, the scanning ISR executes and the program samples the tunneling current signal from the transimpedance amplifier. After averaging five samples, the program compares this average to the set point value to find the error. This error value is used to calculate the voltage to output to the z piezoelectric tube. The error value and the average value are concatenated and placed in a queue. The last task of the scanning ISR is to output the voltage to the x and y piezoelectric tubes. In between execution of the scanning ISR, the computer sends data through the dual port memory to the host computer via a double buffered system. The data in the queue is emptied into the first of two buffers. When this buffer is full, the DSP signals the host computer to read the data out of the buffer. While the host computer reads the data, the DSP is writing data to the second buffer. When the second buffer is full, the DSP signals the computer to read out of this buffer. At this point the DSP starts filling the first buffer again. With this system no data is lost by being overwritten by the DSP.

User Interface and Image Display

Visual Basic was the language used for creating the graphical user interface. This interface acts as a front end to the DAC and the program that the DSP uses. Several windows allow access to different functions of the program. The main window is the control panel (Figure 20). Through this control panel the user can set all of the

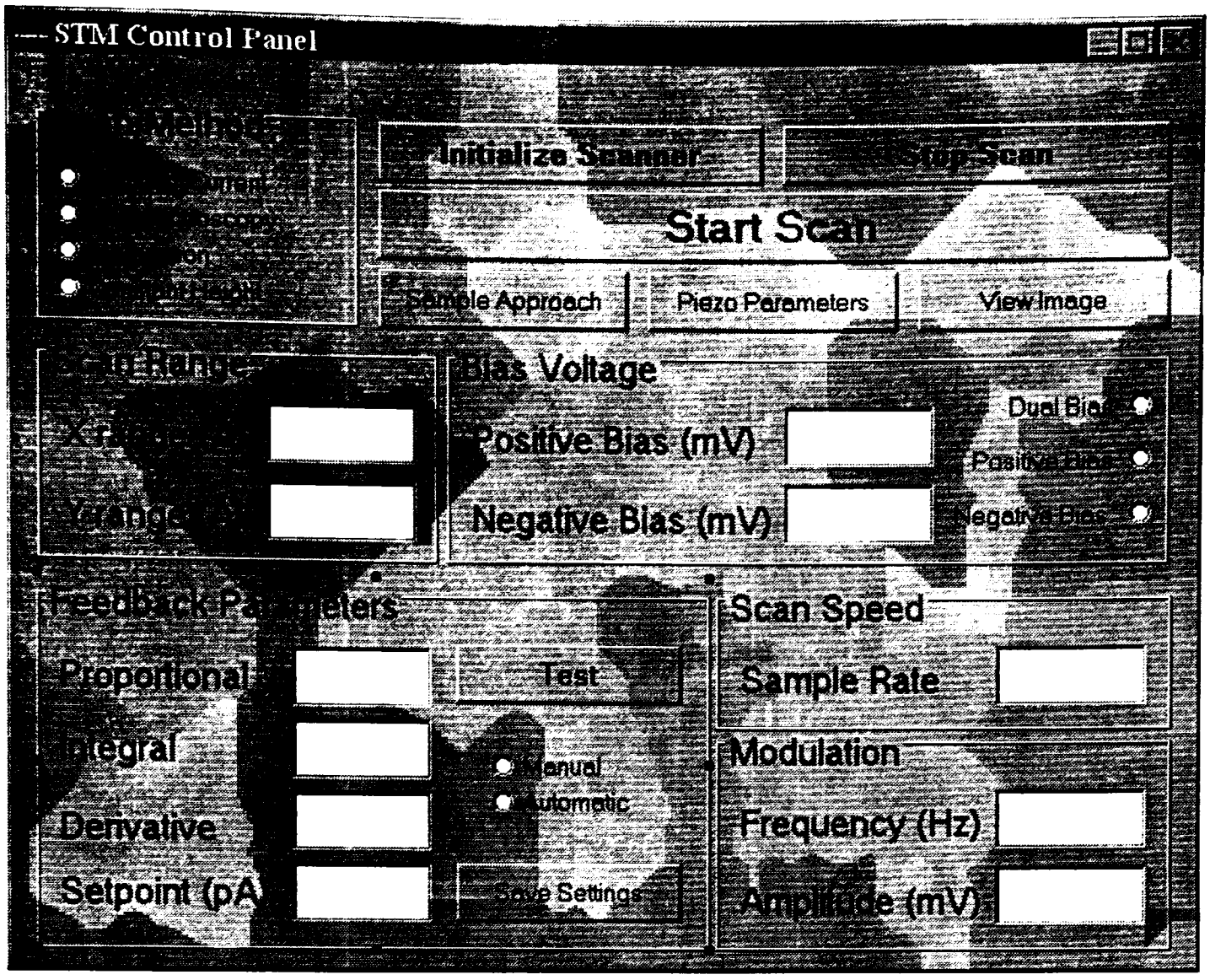

Figure 20. STM Control Panel Window

parameters needed to operate the microscope. Furthermore, the user can access the other windows, such as the coarse positioning window. All of the parameters the user enters can be saved into a file and automatically loaded when the user runs the program.

Using Visual Basic to program the interface simplifies the creation of windows; but accessing hardware or physical memory locations is difficult or impossible. This problem makes retrieving data in real time from the DAC very difficult. Visual Basic is capable of using functions in dynamic link libraries (DLLs) and the DLL provided with the PC32 DAC has a number of useful functions; but all of these functions require using physical hardware addresses and memory locations. To solve this problem, a custom

Windows DLL was written in C so that the image data could be transferred from the DAC to the screen and a file on disk. This C library talks directly to the PC32 card and collects the information from the dual port memory. After the DSP program signals the computer that the dual port memory buffer is full, the DLL reads both the tunneling current data and the error data from memory and places these values into two different files—one for the tunneling current data and the other for the error data. The DLL is doing two other tasks while reading in the data. First, the DLL is sorting the samples to find the maximum value. For the second task, the DLL is writing the sample data to the screen so that the user can see the scan data being acquired.

A typical sequence of events for using the interface proceeds as follows. First, the user initializes the DSP card by pressing the "Initialize Scanner" button on the STM control panel. This command initializes the DAC and loads the DSP program into the card. At this point, the DSP program is waiting for a command from the user interface. The default parameters for the scanner are automatically loaded when the STM control panel initiates. Now the user is ready to use the coarse positioning system. Pressing the "Coarse Positioning" button opens the window (Figure 21) to access this function in the DSP program. In this window the amplitude and frequency of the waveform can be set. The user can select to move the sample stage forward towards the tunneling probe. Or the user can select "reverse" to move the stage away from the tunneling probe. The coarse positioning function in the DSP reads the tunneling current as the stage is being translated. If the current exceeds the set point value the function stops to avoid crashing

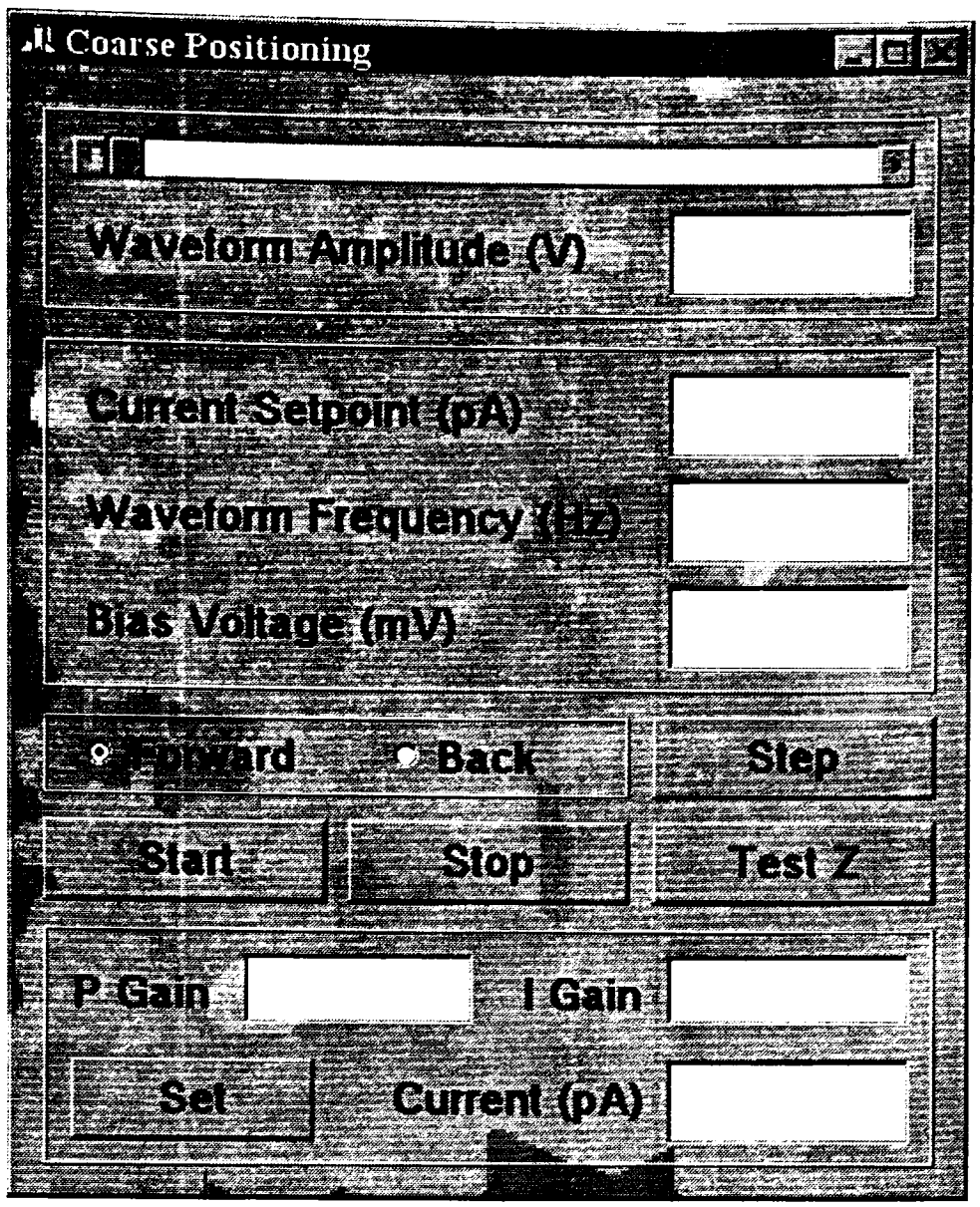

Figure 21. Coarse Positioning Window

the sample into the probe. Once the sample stage is in range for tunneling to occur the user can activate the feedback by pressing the "Test Z" button. This activates the feedback loop. The current is continually displayed in the lower right hand corner of the window. If satisfied with the stability of the tunneling current, the user can begin the scan by pressing the "Start Scan" button on the control panel. As the data is acquired it is displayed on the screen. After the scan is done, the user can save the data and then enlarge and scale the image. Figure 22 shows an image display window after the data has

been scaled. The scan parameters are displayed to the right of the image and the image filename is displayed in the window title bar.

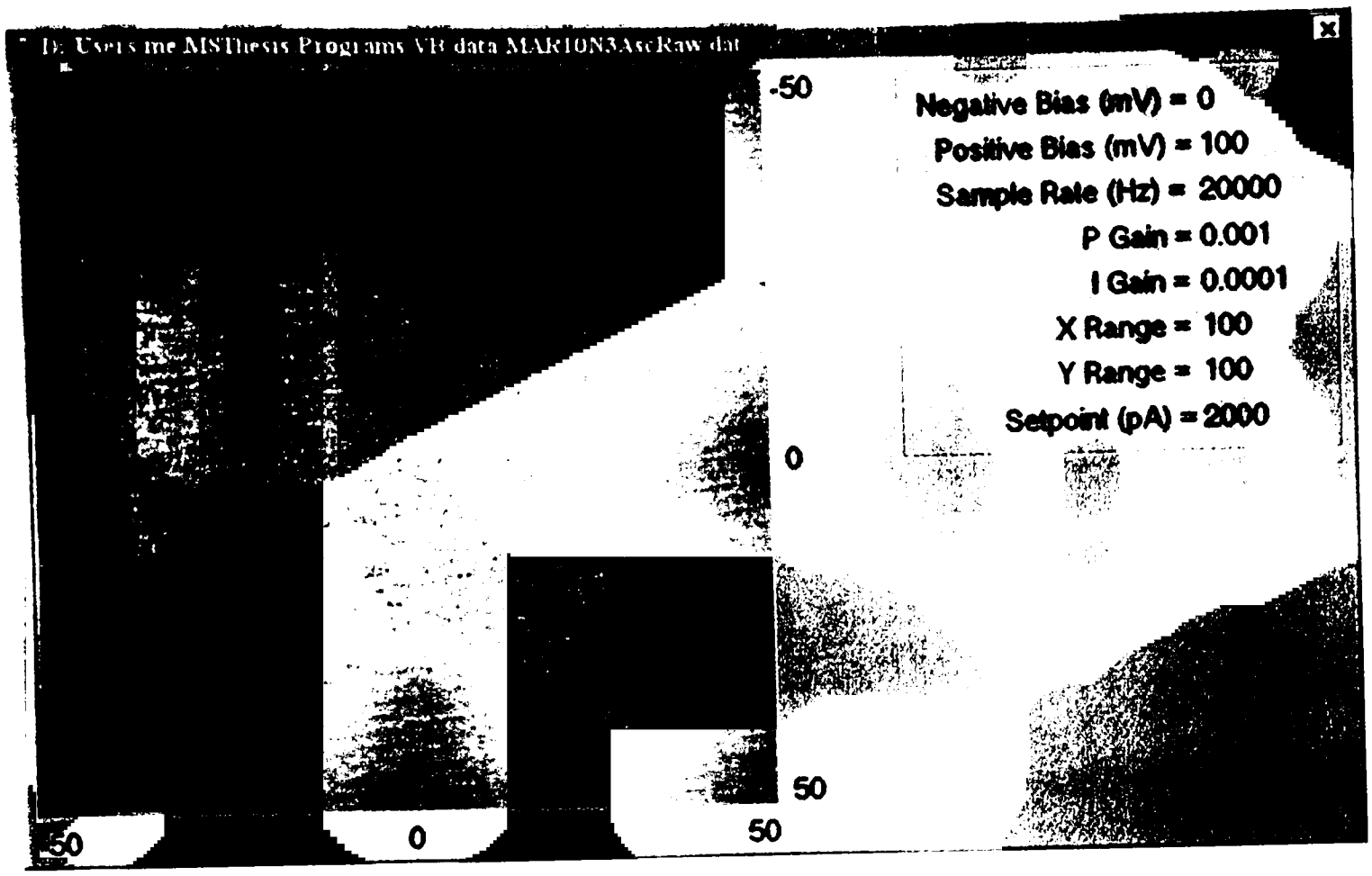

Figure 22. Image Display Window

CHAPTER IV

CARBON NANOTUBES

Carbon nanotubes, also known as tubular fullerenes, are cylindrical graphene sheets of sp^2-bonded carbon atoms.[31] Previous STM and AFM studies of these nanotubes have measured various properties of carbon nanotubes. These nanotubes are single molecules measuring a few nanometers in diameter and several microns in length (Figure 23). Sumio Iijima discovered carbon nanotubes in 1991. He was making C_{60} molecules with the carbon arc process. In the same soot as the C_{60} molecules, he found carbon nanotubes. Since then, fabrication methods have been optimized to produce nanotubes in yields higher than 70 percent.[32]

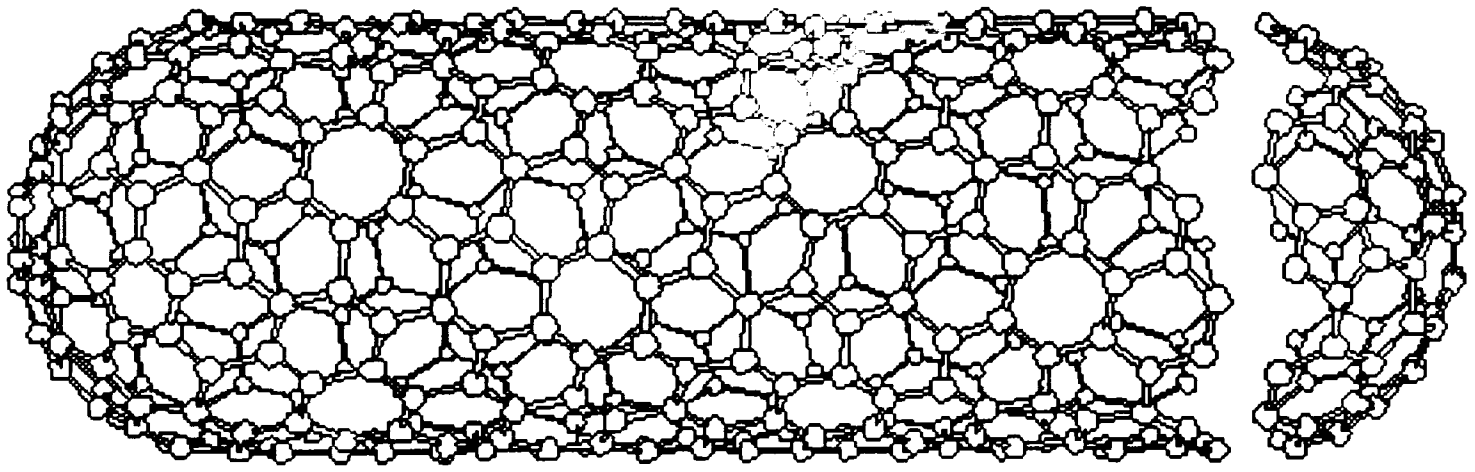

Figure 23. Carbon Nanotube[33]

Carbon nanotubes come in a variety of diameters and lengths. Depending on the growth process, the length of the tubes can be from approximately 100 nanometers to several microns. Diameters vary from 1 to 20 nanometers. Another parameter describing

carbon nanotubes is their chiral angle. This angle is specified by how the graphene sheet is rolled into a cylinder (Figure 24). By convention, a nanotube with its axis collinear with the horizontal ($\theta = 0$) line in Figure 24 is called a "zigzag" nanotube. This name derives from the appearance of the half-fullerene molecule that can cap the end of the

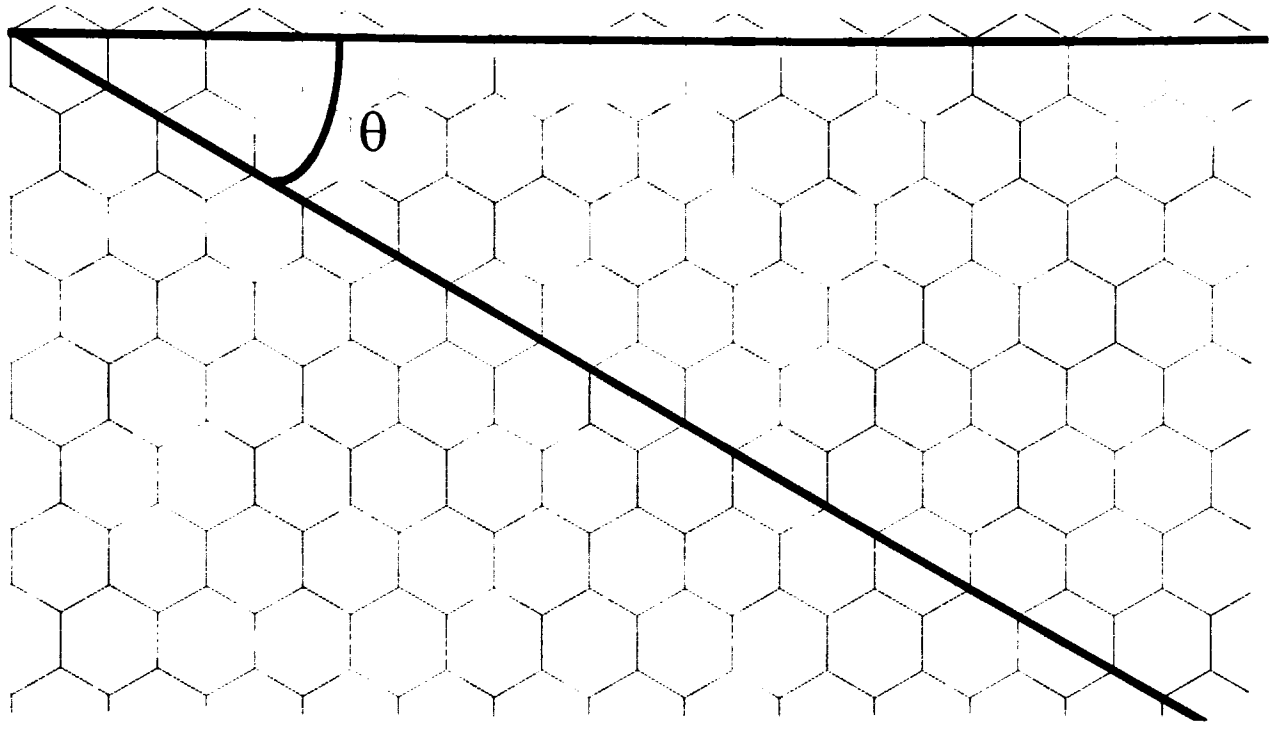

Figure 24. Chiral Angle Theta

tube. Nanotubes can form with axes collinear to several lines forming chiral angles from 0 to 30 degrees. The number of unique end caps for each possible chiral angle depends on the diameter of the nanotube.

Properties

Being one giant molecule, carbon nanotubes have unusual mechanical and electrical properties. The conductivity of single-wall carbon nanotubes can vary from semi-conductive to metallic depending on the chiral angle of the tube and its diameter.

The mechanical properties of nanotubes are also unusual. Numerical simulations predict the Young's modulus of single wall nanotubes to be in excess of a terapascal. Transmission electron microscope (TEM) photographs have shown individual nanotubes bent into a radius of curvature of less than 20 nanometers.

Fabrication Methods

Various techniques are capable of synthesizing carbon nanotubes. The carbon arc method, used initially for producing C_{60} fullerenes, is the most common and perhaps easiest way to produce carbon nanotubes. Chemical vapor deposition in an apparatus used for creating vapor grown carbon fibers has also produced carbon nanotubes. Finally, laser vaporization of a carbon block has produced the most uniform single wall carbon nanotubes. The carbon arc method was employed in the procedure described here and thus discussion will focus on this method specifically.[34]

Initially, the carbon arc method was developed to produce C_{60} fullerenes. This method creates nanotubes through the arc-vaporization of two carbon rods placed end to end separated by approximately 1mm. A direct current of 50 to 100 A driven by approximately 20 V creates a high temperature discharge between the two electrodes. The discharge vaporizes one of the carbon rods and forms a small rod shaped deposit on the other rod. Producing nanotubes in high yield depends on the uniformity of the plasma arc and the temperature of the deposit formed on the carbon electrode.

The laser vaporization method produces single wall carbon nanotubes in high yields. A graphite target is heated to 1200 °C in a quartz tube. A Nd-YAG laser ablates

carbon off of this graphite target. At the end of the furnace a water cooled brass cone collects the soot from the ablation. This soot contains a high percentage of single wall carbon nanotubes.

Two theories concerning the growth mechanism for tubular fullerenes are currently under debate. The first assumes that the nanotubes are always capped and C_2 molecules are absorbed at the pentagonal defects at the caps. The second method assumes that the nanotubes are open during the growth process and carbon molecules are added to the open ends of the nanotubes.

The growth mechanism in the arc discharge method is believed to be the open tube method. Absorption of a single C_2 dimer at an active dangling bond adds one hexagon to the open end. The sequential addition of C_2 dimers results in continuous growth of the nanotube. What keeps the nanotube open-ended is unknown, creating a serious problem for this model. One suggestion is the high electric field in the region of tube growth. In the carbon arc method the voltage between the electrodes is generally on the order of 20 volts. A 1 mm separation distance creates an electric field of 20000 V/m. But the temperatures involved ionize the carbon atoms, thus creating some shielding from the electrodes. This may reduce the effective separation distance to a few microns subsequently increasing the field strength. A field this high could prevent the closure of the nanotube ends.

CHAPTER V

RESULTS

The various systems comprising the scanning tunneling microscope have been tested. For the electrical instrumentation, the tunneling current amplifier has been tested with a Keithley electrometer and a constant current source. The transimpedance amplifier has been calibrated to measure 16 nA at a ten-volt output corresponding to the full scale input on the A/D converter. The amplifier has about 20 mV of noise that corresponds to approximately 30 pA of current noise. Currently, a generic replacement opamp, the ECG937, is being used in the transimpedance amplifier instead of the AD549. This opamp is the source of most of this noise.

The piezoelectric drive amplifiers have been tested and have a bandwidth of approximately 10 kHz with less than 5 mV of rms noise. With the calculated sensitivity of the piezoelectric scanning tube being approximately 243 Å/V, the motion of the tip is approximately 1.2 Å. This motion may be too high for atomic resolution to be achieved. For the piezoelectric tube that maintains the probe-sample distance, the sensitivity is calculated to be approximately 43 Å/V. With this value the probe-sample separation cannot be maintained to better than .2 Å. This level of precision is adequate for maintaining a low tunneling current where the probe is relatively far from the sample.

Several tunneling probes have been fabricated via electrochemical etching. These probes are very sharp. At 1200 magnification under an optical microscope, no radius of

curvature could be seen. With a scanning electron microscope at 2500 magnification the radius of curvature of the tip was estimated to be less than 1 micron.

The feedback and control system can maintain a stable tunneling current from 100 pA to 15 nA. The stability of the tunneling current is very sensitive to the condition of the tunneling probe. Short dull probes can produce very stable tunneling currents; but these probes are not sharp enough to produce atomic resolution. Very sharp probes are susceptible to vibration, causing the tunneling current to be unstable. In any case, the stability of this current decreases with increasing bias voltage. The user interface is capable of testing the step response of the feedback and control system. For slow "constant height" scans the proportional gain should be about 10 times the integral gain.

The vibration isolation system dampens any vibrations originating in the floor. Vibrations produced on the table are visible in the tunneling current signal. A more serious problem results from acoustic coupling. The electric fans used to cool the piezoelectric drive amplifiers produce unacceptable levels of 60 Hz vibrations. These vibrations appear as horizontal lines in the image.

The coarse positioning system can reliably move the sample stage toward or away from the tunneling probe. The user can select wave amplitudes from 1 to 100 volts at frequencies from 1 to 300 Hz. Single stepping the coarse approach mechanism is also possible. The amplitude and period of the single steps is adjustable over the same ranges as the continuous stepping. A maximum translation speed for the sample stage was measured at approximately .11 mm/second.

By measuring the sample translation speed for different wave amplitudes at a constant frequency, a rough estimate of the piezoelectric tube sensitivity can be found. For three different wave amplitudes, 100 V, 75 V, and 50 V, the time required for translating the stage over a 6 mm distance was measured. The frequency of all three amplitudes was 300 Hz. Assuming the number of translation steps is equal to the frequency, the total number of steps required to move 6 mm can be found by multiplying the frequency by the total time of translation. For the 100 V wave a step size of .38 microns was found. For the 75 V wave the step size was .29 microns. The 50 V wave had a step size of .12 microns. By dividing these step sizes by their respective amplitudes the values in Å/V can be found. The average of these three values was approximately 34 Å/V. This value is lower than the 43 Å/V calculated via equation 18. But the sensitivity of the piezoelectric tubes decreases with age in a logarithmic fashion. With a 3 percent decrease[35] per decade of time, and the age of these piezoelectric materials being over a year, the 43 Å/V sensitivity of the piezoelectric is reduced by about 18 percent to approximately 35 Å/V. Assuming the scanning piezoelectric tube has aged in a similar manner, the sensitivity of this tube changes from 243 Å/V to approximately 200 Å/V.

Numerous test scans of highly oriented pyrolytic graphite (HOPG) have been taken. This sample was used because it has a known nearest neighbor distance of about 2.5 Å. Furthermore, this material can be cleaved very easily to expose a smooth surface of material that remains clean for extended periods of time. Figure 25 shows a scan of HOPG. No surface features are discernible. Other image artifacts are present which reveal problems in the system. The lines in the image slanting upwards and to the right

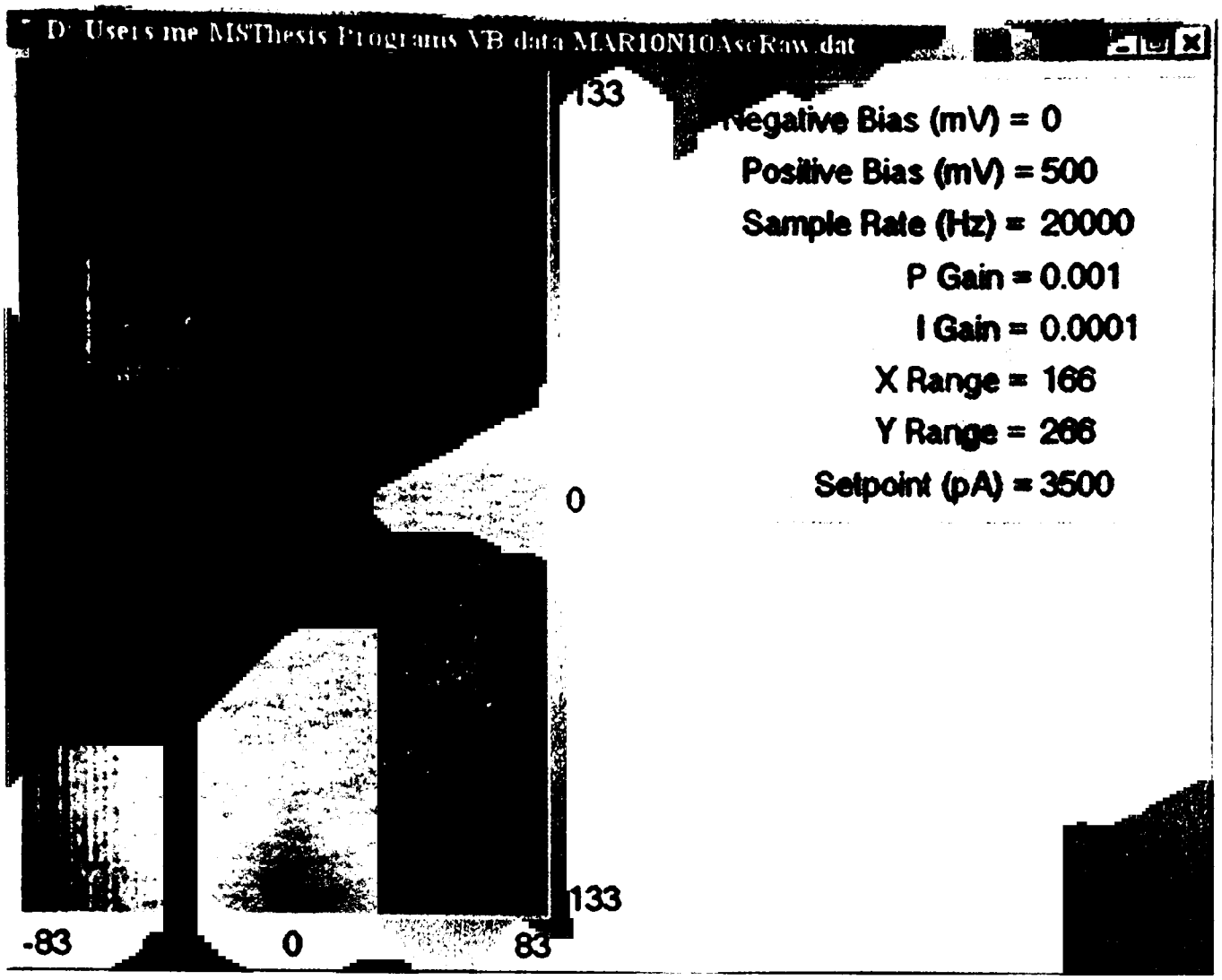

Figure 25. HOPG Scan

are from 60 Hz noise in the system. On the left side of the image the dark band and vertical lines are due to the slow reaction of the feedback and control system when the raster signal moves the tunneling probe from the right side of the scan area to the left side. This problem has been fixed by changing the manner in which the scans are acquired. Instead of scanning every line from left to right, alternate lines are scanned right to left. With this method, no large jumps in the lateral position of the probe occur causing discontinuities in the operation of the feedback system.

With the new scanning system, the artifacts on the left side of the image are gone. Better vibration isolation has also been achieved by simply removing the system

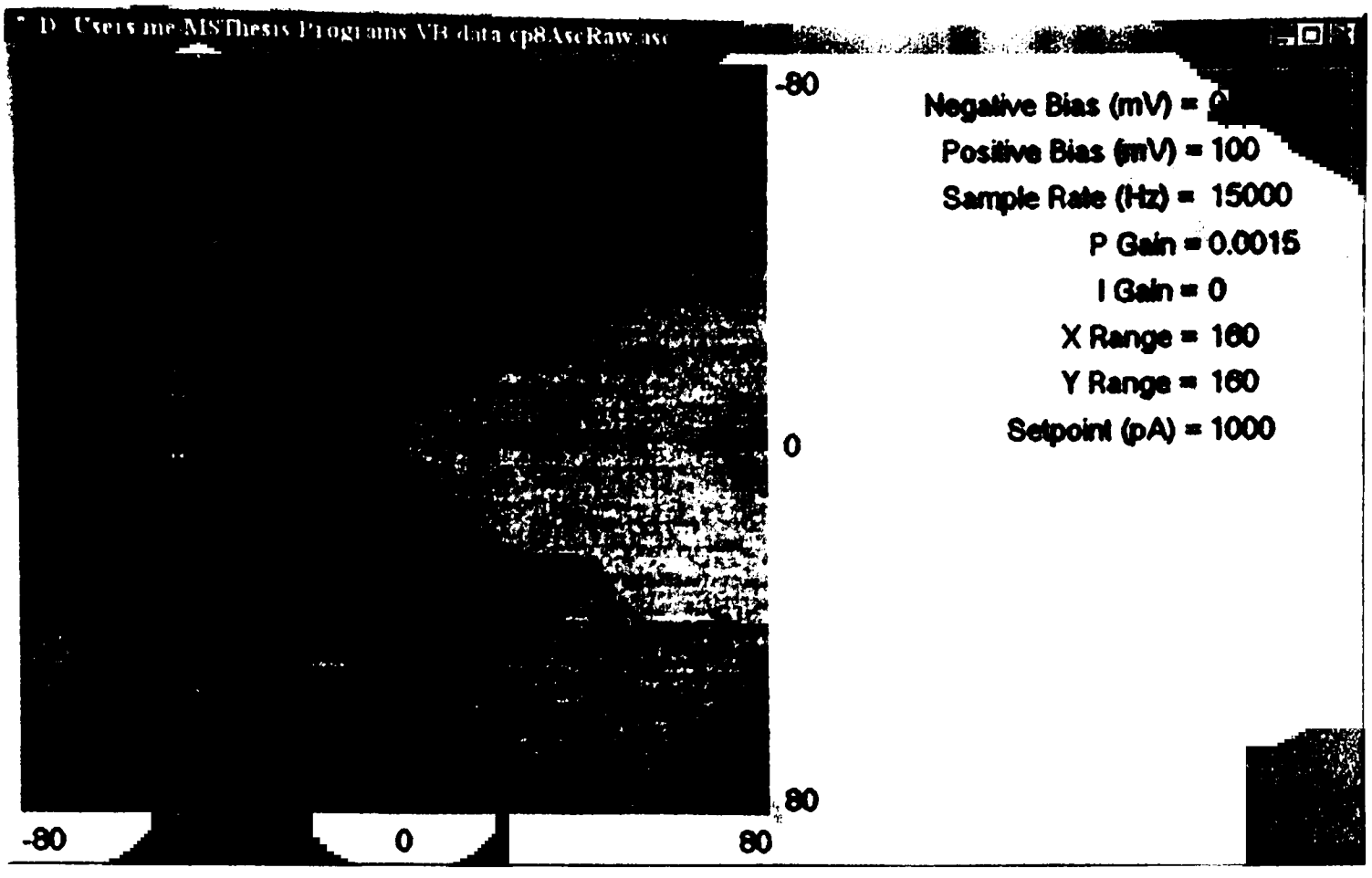

Figure 26. Smaller HOPG Scan

computer from the STM table. Figure 26 shows a scan of HOPG with the new raster system and the improved vibration isolation.

No atomic features are visible in this image. Several problems may be responsible for the lack of atomic resolution. The scanning tube sensitivity of approximately 200 Å/V and electrical noise of about 5 mV creates effectively 1 Å of noise in the position of the probe. The 2.4 Å distance may not be visible with this much noise. The image data may be lost in the vibrational noise of the probe with respect to the sample. These vibrations translate into unwanted noise in the tunneling current.

Reducing the sensitivity of the piezoelectric tubes by driving them in unipolar mode allows for scans with atomic resolution. Driving the piezoelectric tubes in unipolar mode reduces the effective noise in the position of the tunneling probe to about .5 Å.

Figure 27 shows a scan of HOPG with the piezoelectric tubes in unipolar mode. The lower two thirds of the image shows atomic features.

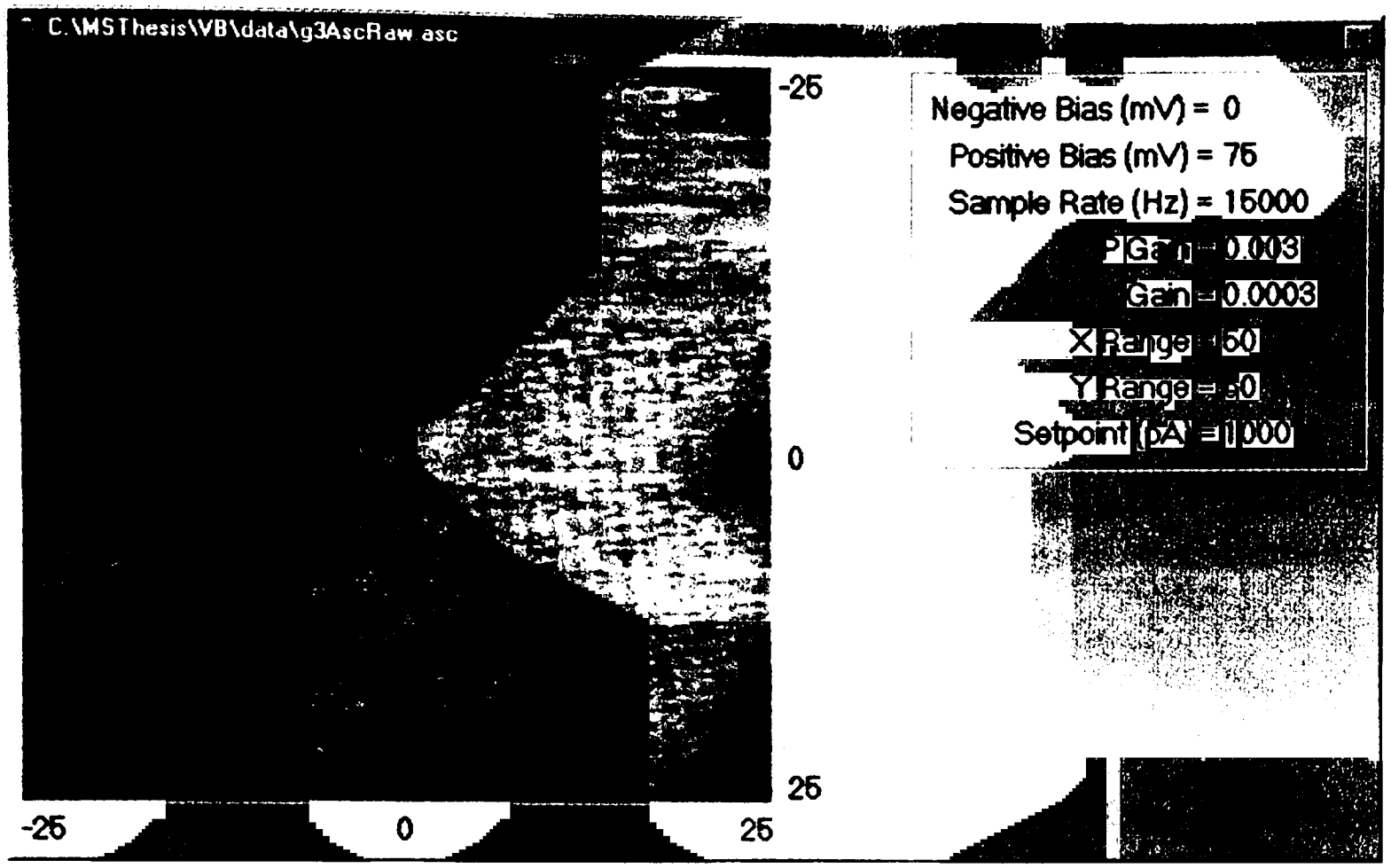

Figure 27. HOPG Scan Showing Atomic Resolution

The size of carbon nanotubes is large compared to the resolution limits created by problems related to noise. But, no nanotubes have been imaged due to limitations in the file size of the scanned images. Currently, the scan system takes data at every increment of the D/A converter. For example, with this setup, an image 100 nm by 100 nm contains over 2.6 million data points. With each data point being 2 bytes, this results in image files of over 5 megabytes. Manipulating and viewing this much data is time consuming.

CHAPTER VI

CONCLUSIONS

A scanning tunneling microscope has been built. The initial tests of the microscope show promising results; but many improvements are necessary. Some simple improvements are currently being implemented. The piezoelectric amplifiers have been altered to drive the scanning tube in unipolar mode, effectively reducing the tube sensitivity by a factor of two. Even with this adjustment, the maximum scan area is still approximately $1\mu m^2$. For larger scans, the amount of data is being limited to 512 by 512 points. This limitation will allow large areas to be scanned quickly. Furthermore, the images produced by these scans will be of a manageable size.

Rebuilding the microscope head is a major task that may improve many aspects of performance. Using less sensitive piezoelectric tubes of a smaller geometrical size reduces the microscope sensitivity to electrical noise and ambient vibration. Furthermore, although more difficult to implement, other designs allow coarse positioning in all three directions. The "beetle type" STM invented by Besocke[36] enables coarse positioning in three dimensions.

REFERENCES

1. G. Binnig, H. Rohrer, Ch. Gerber, E. Weibel, "Surface studies by scanning tunneling microscopy," *Phys. Rev. Lett.* v49 n1, pp. 57-61, (1982).

2. Joseph A. Stroscio, William J. Kaiser, *Scanning Tunneling Microscopy*, Academic Press, San Diego, pp. 149-150, (1993).

3. Joseph A. Stroscio, William J. Kaiser, *Scanning Tunneling Microscopy*, Academic Press, San Diego, p. 5, (1993).

4. C. Julian Chen, *Introduction to Scanning Tunneling Microscopy*, Oxford, p. 53, (1993).

5. C. Julian Chen, *Introduction to Scanning Tunneling Microscopy*, Oxford, p. 64, (1993).

6. J. Bardeen, "Tunneling from a many body point of view," *Phys. Rev. Lett.* v6 n2, pp. 57-59, (1960).

7. C. Julian Chen, *Introduction to Scanning Tunneling Microscopy*, Oxford, p. 65, (1993).

8. Joseph A. Stroscio, William J. Kaiser, *Scanning Tunneling Microscopy*, Academic Press, San Diego, p. 7, (1993).

9. C. Julian Chen, *Introduction to Scanning Tunneling Microscopy*, Oxford, p. 9, (1993).

10. C. Julian Chen, *Introduction to Scanning Tunneling Microscopy*, Oxford, p. 28, (1993).

11. C. Julian Chen, *Introduction to Scanning Tunneling Microscopy*, Oxford, pp. 213-214, (1993).

12. Morgan Matroc, Inc., *A Guide to Modern Piezoelectric Ceramics*, p. 4, (1997).

13. C. Julian Chen, *Introduction to Scanning Tunneling Microscopy*, Oxford, p. 235, (1993).

14. G. Binnig, and D. P. E. Smith, "Single-tube three-dimensional scanner for scanning tunneling microscopy," *Rev. Sci. Instrum.* v57, pp. 1688-1689, (1986).

15. Morgan Matroc, Inc., *A Guide to Modern Piezoelectric Ceramics*, p. 10, (1997).

16. C. Julian Chen, *Introduction to Scanning Tunneling Microscopy*, Oxford, p. 230, (1993).

17. G. Binnig, H. Rohrer, Ch. Gerber, E. Weibel, "Surface studies by scanning tunneling microscopy," *Phys. Rev. Lett.* v49 n1, pp. 57-61, (1982).

18. H. Bourque, R. M. Leblanc, "Electrochemical fabrication of scanning tunneling microscopy tips without an electronic shut-off control," *Rev. Sci. Instrum.* v66 n3, pp. 2695-2697, (1995).

19. J. W. Lyding, S. Skala, J. S. Hubacek, R. Brockenbrough, G. Gammie, "Variable-temperature scanning tunneling microscope," *Rev. Sci. Instrum.* v59 n9, pp. 1897-1902 (1988).

20. B. J. McIntyre, M. Salmeron, and G. A. Somorjai, " A variable pressure/temperature scanning tunneling microscope for surface science studies," *Rev. Sci. Instrum.* v64 n3, pp. 687-691, (1993).

21. F. Besenbacher, E. Lægsgaard, K. Mortensen, U. Nielsen, and I. Stensgaard, "Compact, high-stability, 'thimble-size' scanning tunneling microscope," *Rev. Sci. Instrum.* v59 n7, pp. 1035-1038, (1988).

22. S. Kleindiek and K. H. Herrmann, "A miniaturized scanning tunneling microscope with a large operating range," *Rev. Sci. Instrum.* v64 n3, pp. 692-693 (1993).

23. F. Mugelem Ch. Kloos, P. Leiderer, R. Moller, "A simple, ultrahigh vacuum compatible scanning tunneling microscope for use at variable temperatures," *Rev. Sci. Instrum.* v67 n7, pp. 2557-2559, (1996).

24. D. W. Pohl, "Dynamic piezoelectric translation devices," *Rev. Sci. Instrum.* v58 n1, pp. 54-57, (1987).

25. Ch. Renner, Ph. Niedermann, A. D. Kent, and Ø. Fischer, "A vertical piezoelectric inertial slider," *Rev. Sci. Instrum.* v61 n3, pp. 965-967, (1990).

26. Henry W. Ott, *Noise Reduction Techniques in Electronics Systems*, Wiley-Interscience, New York, p. 200, (1976).

27. C. Julian Chen, *Introduction to Scanning Tunneling Microscopy*, Oxford, p. 255, (1993).

28. Apex Microtechnology, *Application Notes*, (1994).

29. Innovative Integration, *PC32 Hardware Reference Manual*, p. 26, (1995).

30. David R. Baselt, Steven M. Clark, Michael Youngquist, Charles, Spence, John D. Baldeschwieler, "Digital signal processor control of scanning probe microscopes," *Rev. Sci. Instrum.* v64 n7, pp. 1874-1882, (1993).

31. Dresselhaus, M. S., G. Dresselhaus and P. C. Eklund, *Science of Fullerenes and Carbon Nanotubes*, Academic Press, San Diego, p. 756, (1996).

32. Boris I. Yakobson, Richard Smalley, "Fullerene Nanotubes: $C_{1,000,000}$ and Beyond," *American Scientist*, Volume 85, pp. 324-337, July-August 1997.

33. Dresselhaus, M. S., G. Dresselhaus and P. C. Eklund, *Science of Fullerenes and Carbon Nanotubes*, Academic Press, San Diego, p. 758, (1996).

34. T. W. Ebbesen and P. M. Ajayan, "Large-scale synthesis of carbon nanotubes," *Nature* v358, pp. 220-222, (1992).

35. Morgan Matroc, Inc., *A Guide to Modern Piezoelectric Ceramics*, p. 11, (1997).

36. K. Besocke, "An easily operable scanning tunneling microscope," *Surface Science* v181, pp. 145-153, (1987).

APPENDIX

SOURCE CODE

```
/*************************************************************
*  Program: Action.c
*  Purpose: This is the main DSP program for the scanning tunneling
*  microscope. This program is initiated by the host PC and then waits
*  until it receives the appropriate code from the PC to begin
*  execution. Each code corresponds to a different procedure for the
*  program. I'm using numerical codes instead of passing characters
*  because it's easier.
*  Code:      Function:
*  9999       Sample Approach routine. The host PC sends this
*             command when the sample approach routine is to be
*             used. Generally this will be used all of the time.
*  9876       This code is sent to the host PC from the DSP card to
*             notify the host PC to clear the mailboxes for
*             receiving address data.
*
*  8888       Scanning with feedback incorporated. This routine
*             basically consists of one ISR to do feedback and
*             control.
*
*  7777       Exit the program
*
*  6789       Data Ready.  This code is sent to the host PC DLL
*             program to notify this DLL the it can read the data
*             from the given offset address.
*
*  6666       I-V Spectroscopy. Probably won't be implemented for a
*             while.
*
*  5555       Modulation technique. See I-V Spectroscopy.
*
*  4444       Feedback parameter adjustment
*
*  3333       This code tells the PC that the scan is done. Usually
*             the integer Pcstop is set to 3333 somewhere by the
*             program.
*
*  2222       Fine adjustment of the tunneling distance.
```

```
*
**********************************************************************/
#include "stdio.h"
#include "periph.h"
#include "math.h"
#include "time.h"

#define fdbk_and_ctrl_isr       c_int99
#define fdbk_test_isr           c_int90
#define sample_approach_isr     c_int80
#define adjust_isr              c_int89
#define INTERRUPT 8

#define resolution 250
int prev;
int halfres;

/* data buffer pointers (in dual port ram) */
#define BUF_LENGTH 0x150
volatile int offset;
volatile int *dpram = DPRAM;
int Pcstop;

/* Mailbox prototypes and such.*/
long read_Terminal_mailbox(void);
void write_Terminal_mailbox(long);
long read_Monitor_mailbox(void);
void write_Monitor_mailbox(long);
struct mailbox* Term_MAILBOX;
struct mailbox* Mon_MAILBOX;
int Term_mailbox_semaphore;
int Mon_mailbox_semaphore;

/* ISR data queue */
#define QSIZE  0x2500
volatile int queue[QSIZE];
volatile int head, tail;
void datashuffle(void);

/* Feedback and control variables */
void fdbk_and_ctrl_isr();
float Setpoint;
int scan_freq;
```

```
float Pc;
float Ic;
float a;
float b;
float sample;

float dacconvert;
float err;
float er1;
float zc;
float zc1;
int s;
float avesample;
float sumsample;

/* Data queues for data collection and shuffling to the DSP */
static inline int enqueued(void);
static inline void enqueue(int value);
static inline int dequeue(void);

/* Sample Approach variables */
void sample_approach_isr();
int sample_approach_freq;
float tc;
int sample_approach[resolution];
float sample_approach_amp;
int approach_done;
int sample_approach_direction;
int alpha;
int tcout;
float step;
float temp;
int single_step;

void adjust_isr();
void fdbk_test_isr();

int data_ready;
int queue_empty;

int value;
int i;
int bias;
```

```
int scan_done;
float pzgain;
int pause;
float tigain;

int code;
int program_done;
int finished;

/* X and Y Raster variables */
int x_scan_size;    /* scan_size corresponds to the x scan range */
int y_scan_size;    /* scan_size corresponds to the y scan range */
int x_wave;
int y_wave;
int x_wave_start;
int y_wave_start;
int x_wave_end;
int y_wave_end;
int d;
int mx;
int my;

/*  ENQUEUED()
   Returns number of data in A/D queue
*/
static inline int enqueued(void)
{
    int depth = head - tail;

    return((depth < 0) ? (depth + QSIZE) : depth);
}

/*  DEQUEUE()
   Dequeues next A/D element into address
*/
static inline int dequeue(void)
{
    int value = queue[tail++];

    if (tail == QSIZE)
        tail = 0;

    return(value);
```

```
}

/*  ENQUEUE()
   Inserts next element in A/D queue
*/
static inline void enqueue(int value)
{
    queue[head++] = value;
    /* Resetting the queue index */
    if (head == QSIZE)
        head = 0;
}

/*****************************************************************

        FUNCTION: Main

        PURPOSE: Sets up loop for receiving code from host PC.

*****************************************************************/
void main(void)
{
  MHZ = 40;                          /* cpu speed */
timer(0, 0);                         /* Disable timer */

Mon_MAILBOX = (struct mailbox*)(MAILBOXES + 0);
Mon_mailbox_semaphore = 0 + (current_cpu * NUM_MAILBOXES);
Term_MAILBOX = (struct mailbox*)(MAILBOXES + 4);
Term_mailbox_semaphore = 1 + (current_cpu * NUM_MAILBOXES);

/* init variables */
head = tail = 0;
offset = 0;
dacconvert=-3276.70;
pzgain=10.0;
tigain=.625;

enable_interrupts();

program_done=0;

/*
 * Here is the one do loop that controls everything. This loop waits
```

```
* for the computer to send the appropriate code to commence action.
* This loop stops when the variable program_done=1.
*/

do{
 code=read_Terminal_mailbox();   /* Code to determine action. */

 /* Fine adjustment after z positioning */
 if (code==2222){
   code=0;

   Pc = read_Terminal_mailbox()/100000.0;
   Ic = read_Terminal_mailbox()/100000.0;
   Setpoint = read_Terminal_mailbox();
   bias = read_Terminal_mailbox();

   if (bias<0){
     Setpoint=-Setpoint;
   }

   bias = bias*dacconvert/1000.0;

   Setpoint = Setpoint*dacconvert*tigain/1000.0;

finished=0;
pause=0;

a=Pc+Ic;
b=-Pc+Ic;

zc=0;
er1=0;
s=0;
avesample=0.0;
sumsample=0.0;

*DAC3=bias;

install_int_vector(adjust_isr, 9);   /* Install interrupt vector */
enable_interrupt(INTERRUPT);      /* Enable timer interrupts */
timer(0, (int)(20000));

do{
```

```
get_semaphore(Mon_mailbox_semaphore);
pause = Mon_MAILBOX->RCV;
Mon_MAILBOX->ACK = 0;
release_semaphore(Mon_mailbox_semaphore);

if (pause==1){
  disable_interrupt(INTERRUPT);  /* Pause the ISR */
}

if (pause==0){
  enable_interrupt(INTERRUPT);   /* Reinitiate ISR */
}

if (pause==2){
  disable_interrupt(INTERRUPT);
  finished=1;
}
}while(!finished);

timer(0, 0);          /* Disables timer ending isr */

*DAC0=0;
*DAC1=0;
*DAC3=0;
convert();
}

/* Feedback parameter testing */
if (code==4444){
  code=0;

  Pc = read_Terminal_mailbox()/100000.0;
  Ic = read_Terminal_mailbox()/100000.0;
  Setpoint = read_Terminal_mailbox();
  bias = read_Terminal_mailbox();

  bias = bias*dacconvert/1000.0;

  Setpoint = Setpoint*dacconvert*tigain/1000.0;

  finished=0;
  pause=0;
  err=0;
```

```
a=Pc+Ic;
b=-Pc+Ic;

s=0;
avesample=0.0;
sumsample=0.0;

*DAC3=(int)(bias);

install_int_vector(fdbk_test_isr, 9);    /* Install interrupt vector */
enable_interrupt(INTERRUPT);        /* Enable timer interrupts */
timer(0, (int)(20000));

do{
  get_semaphore(Mon_mailbox_semaphore);
  pause = Mon_MAILBOX->RCV;
  Mon_MAILBOX->ACK = 0;
  release_semaphore(Mon_mailbox_semaphore);

  if (pause==1){
    disable_interrupt(INTERRUPT);  /* Pause the ISR */
  }
  if (pause==3){
    Setpoint=Setpoint-2048;  /* 500pA jump for test */
    pause=0;
  }

  if (pause==2){
    disable_interrupt(INTERRUPT);
    finished=1;
  }
 }while(!finished);

 timer(0, 0);          /* Disables timer ending isr */

 *DAC0=0;
 *DAC1=0;
 *DAC3=0;
 convert();
}
```

```
/* This is the sample approach stuff here */
if (code==9999){
  code=0; /* Resetting the code */
  Setpoint = read_Terminal_mailbox();
  sample_approach_freq = read_Terminal_mailbox();
  bias = read_Terminal_mailbox();
  sample_approach_direction = read_Terminal_mailbox();
  sample_approach_amp = read_Terminal_mailbox();
  single_step=read_Terminal_mailbox();

  if (sample_approach_direction==1){
    alpha=1;
  }

  if (sample_approach_direction==0){
    alpha=-1;
    bias=0;  /*Turns off bias for sample removal*/
    Setpoint=16500;
  }

  bias = bias*dacconvert/1000.0;
  sample_approach_amp = sample_approach_amp*dacconvert/pzgain;
  Setpoint = Setpoint*dacconvert*tigain/1000.0;
halfres=resolution/2;
/* This section makes the wavetable for the coarse approach. */
   for (i = 0; i <= halfres; i++){
   step=(float)i/(float)halfres;
   temp=sample_approach_amp-step*step*step*sample_approach_amp;
   sample_approach[i]=(int)temp-(int)sample_approach_amp;
   sample_approach[resolution-i]=(int)temp-(int)sample_approach_amp;
   }

/*initialize variables*/
approach_done=0;
Pcstop=0;
pause=0;
tc=0;
prev=0;

/* Here I set the tip bias on DAC3 */
*DAC3=(int)(bias);
```

```
/* Install interrupt vector and let the timer take over */
install_int_vector(sample_approach_isr, 9);  /* Install int. vector */
enable_interrupt(INTERRUPT);                 /* Enable timer interrupts */
timer(0, (int)(sample_approach_freq*resolution));      /* TIM0 initiates sample
approach */

do{
  get_semaphore(Mon_mailbox_semaphore);
  pause = Mon_MAILBOX->RCV;
  Mon_MAILBOX->ACK = 0;
  release_semaphore(Mon_mailbox_semaphore);

  if (pause==2){
    disable_interrupt(INTERRUPT);
    approach_done=1;
    Pcstop=3333;
  }
}while(!approach_done);

tcout=-(int)((tc)*1000.0/(tigain*dacconvert));
write_Monitor_mailbox(Pcstop);  /* Notifies PC sample approach is done*/
write_Terminal_mailbox(tcout);
tcout=*ADC0;
  timer(0, 0);          /* Disables timer ending approach */

  *DAC0=0;
  *DAC1=0;
  *DAC2=0;
  tcout=*ADC0;
  convert();            /*resets the DACs to zero*/
}

/* Here is the code for the scanning with feedback. */
if (code==8888){
  code=0; /* Resetting the code */

  /*
   * Poll Current SFM Parameters from host PC.
   * This entire operation works through hardware semaphore
   * handshaking.
   */

  x_scan_size = read_Terminal_mailbox();  /* X Scan Size */
```

```
y_scan_size = read_Terminal_mailbox(); /* Y Scan Size */
bias = read_Terminal_mailbox();       /* Tip bias */
scan_freq = read_Terminal_mailbox();   /* Scan Freq */

Pc = read_Terminal_mailbox()/100000.0;         /* Proportional Gain */
Ic = read_Terminal_mailbox()/100000.0;         /* Integral Gain */
Setpoint = read_Terminal_mailbox();    /* Fdbk setpoint */

write_Terminal_mailbox(9876); /* Notifies mail has been read */

bias = bias*dacconvert/1000.0;

/* Negative sign makes this the absolute value.*/
Setpoint = Setpoint*dacconvert*tigain/1000.0;

mx=1;
my=1;

if (abs(x_scan_size)>511){
  mx=2;
}

if (abs(y_scan_size)>511){
  my=2;
}

/* Initializing raster values for x and y */
x_wave_start=x_scan_size/2;
x_wave_end=-x_wave_start;
y_wave_start=y_scan_size/2;
y_wave_end=-y_wave_start;
x_wave=x_wave_start;
y_wave=y_wave_start;

a=Pc+Ic;
b=-Pc+Ic;

data_ready=6789;
scan_done=0;
queue_empty=0;
Pcstop=0;
err=0;
avesample=0;
```

```
sumsample=0;
s=0;
d=1;

/* Here I set the tip bias on DAC3 */
*DAC3 = bias;

/* Install the interrupt vectors and let the timer take over */
install_int_vector(fdbk_and_ctrl_isr, 9);  /* Install int. vector */
enable_interrupt(INTERRUPT);     /* Enable timer interrupts */
timer(0, scan_freq);       /* TIM0 initiates scan */

datashuffle();

/* Tell the PC the scan is done. */
write_Terminal_mailbox(Pcstop);
timer(0, 0);    /* Disables the timer and ends the scan */

*DAC0=0;
*DAC1=0;
*DAC2=0;
*DAC3=0;
convert(); /*resets the DACs to zero*/
   }

   /* This section exits the program. */
   if (code==7777){
     code=0;

     *DAC0=0;
     *DAC1=0;
     *DAC2=0;
     *DAC3=0;
     convert(); /*resets the DACs to zero*/

     program_done=1;
    }

  }while(!program_done);
}

/*  This is the feedback and control ISR. Actually this ISR does almost
*   everything that needs to be done in the scan mode of operation. The
```

```
*  reason I set the code up this way was so the feedback and control
*  routine would be executed every time data was collected. This ISR
*  starts by reading in data from the ADC into the queue. If the queue
*  is full the code writes the queue to dual port ram and interrupts
*  the PC. The offset address is written to the mailbox and the
*  computer reads the data starting at offset. The feedback and control
*  calculations are done next. The computer implements PI control. To
*  perform the calculations the computer reads the ADC value that was
*  just sampled.
*/
#pragma linkage convention=interrupt
void fdbk_and_ctrl_isr()
{
  sample=(float)(((*ADC0)<<16)>>16);
  sumsample=sumsample+sample;

  if (s==4){
    er1=err; /*er1 is the error value from last sample */
    zc1=zc;
    s=-1; /* Set to -1 so it will be 0 after the s++ below. */
    avesample=sumsample/5.0;
    sumsample=0.0;
/* Do Feedback Calculations */

err=avesample-Setpoint;

zc=zc1+a*err+b*er1;

enqueue((int)avesample<<16|(int)err&0xffff);

/* write to z signal to DAC */
*DAC2 = (int)zc;

/* x and y signal to DACs */
*DAC0=x_wave;
*DAC1=y_wave;

x_wave=x_wave+d;

if (x_wave > x_wave_end){
  d=-1;
  x_wave=x_wave_end;
```

```
      y_wave=y_wave+1;
    }

    if (x_wave < x_wave_start){
      d=1;
      x_wave=x_wave_start;
      y_wave=y_wave+1;
    }

    if (y_wave >= y_wave_end){
      scan_done=1;
      Pcstop=3333;  /* offset will never be this value */
    }
  }
  s++;
}

/* Feedback test isr */
#pragma linkage convention=interrupt
void fdbk_test_isr()
{
   sample=(float)(((*ADC0)<<16)>>16);
   sumsample=sumsample+sample;

if (s==4){
  er1=err;
  zc1=zc;
  s=-1; /* Set to -1 so it will be 0 after the s++ below. */
  avesample=sumsample/5.0;
  sumsample=0.0;

  get_semaphore(Term_mailbox_semaphore);
     /* Update transmit mailbox */
  Term_MAILBOX->XMT = (long)avesample;
  Term_MAILBOX->REQ = -1;
  release_semaphore(Term_mailbox_semaphore);

  err=avesample-Setpoint;

  zc=zc1+a*err+b*er1;

  if (zc >= 22936.0 || zc<=-22936.0){
    timer(0,0);
```

```
        }
        else{
        /* write to z signal to DAC */
        *DAC2 = (int)zc;
        }
      }
      s++;
}

/* Sample approach routine */
#pragma linkage convention=interrupt
void sample_approach_isr()
{
  tc = (float)(((*ADC0)<<16)>>16);
  tc = sqrt(tc*tc);
  Setpoint=sqrt(Setpoint*Setpoint);

  if (single_step==1 && prev>=resolution-1){
    disable_interrupt(INTERRUPT);
    approach_done=1;
    Pcstop=3333;
  }

  if (tc > Setpoint) {
    approach_done=1;
    *DAC2=0;
    convert();
    Pcstop=3333;
   }

   if (tc <= Setpoint) {
     if (++prev == resolution){
       prev = 0;
     }
     *DAC2 = alpha*sample_approach[prev];
   }
}

#pragma linkage convention=interrupt
void adjust_isr()
{
   sample=(float)(((*ADC0)<<16)>>16);
   sumsample=sumsample+sample;
```

```
if (s==4){
  er1=err;
  zc1=zc;
  s=-1; /* Set to -1 so it will be 0 after the s++ below. */
  avesample=sumsample/5.0;
  sumsample=0.0;

  get_semaphore(Term_mailbox_semaphore);
    /* Update transmit mailbox */
  Term_MAILBOX->XMT = (long)avesample;
  Term_MAILBOX->REQ = -1;
  release_semaphore(Term_mailbox_semaphore);

  err=avesample-Setpoint;

  zc=zc1+a*err+b*er1;

  if (zc >= 32767.0 || zc<=-32767.0){
    timer(0,0);
  }
  else{
  /* write to z signal to DAC */
    *DAC2 = (int)zc;
    }
  }
  s++;
}

void datashuffle(void)
{
  do{
    queue_empty=0;

    /* Emptying the queue to the host PC */
    if (enqueued() >= BUF_LENGTH){
      for (i = 0; i < BUF_LENGTH; i++)
        dpram[offset + i] = dequeue();

      write_Terminal_mailbox(data_ready);
      write_Terminal_mailbox(2*offset);
      offset ^= BUF_LENGTH;
      queue_empty=1;
```

```
    }
  }while(!scan_done || !queue_empty);
}

/*
*
* read_Terminal_mailbox  returns 32-bit value from the Terminal mailbox
*
*/
long read_Terminal_mailbox(void)
{
  volatile int x, value;

  do{                          /* Poll till rec mailbox full */
    get_semaphore(Term_mailbox_semaphore);
    x = Term_MAILBOX->ACK;
    release_semaphore(Term_mailbox_semaphore);
  }while(!x);

  get_semaphore(Term_mailbox_semaphore); /* Update transmit mailbox */
  value = Term_MAILBOX->RCV;
  Term_MAILBOX->ACK = 0;
  release_semaphore(Term_mailbox_semaphore);
  return((long)value);
}

/*
*
* read_Monitor_mailbox  returns 32-bit value from the Monitor mailbox
*
*/
long read_Monitor_mailbox(void)
{
  volatile int x, value;

  do{                          /* Poll till rec mailbox full */
    get_semaphore(Mon_mailbox_semaphore);
    x = Term_MAILBOX->ACK;
    release_semaphore(Mon_mailbox_semaphore);
  }while(!x);

  get_semaphore(Mon_mailbox_semaphore);  /* Update transmit mailbox */
```

```
  value = Mon_MAILBOX->RCV;
  Mon_MAILBOX->ACK = 0;
  release_semaphore(Mon_mailbox_semaphore);

  return((long)value);
}

/*
*
* write_Terminal_mailbox  writes 32-bit value to the Terminal mailbox
*
*/
void write_Terminal_mailbox(long value)
{
  volatile int x;

  do{
    get_semaphore(Term_mailbox_semaphore);
    x = Term_MAILBOX->REQ;          /* Poll till mailbox empty */
    release_semaphore(Term_mailbox_semaphore);
  }while(x);

  get_semaphore(Term_mailbox_semaphore);
        /* Update transmit mailbox */
  Term_MAILBOX->XMT = (long)value;
  Term_MAILBOX->REQ = -1;
  release_semaphore(Term_mailbox_semaphore);
}

/*
*
* write_Monitor_mailbox  writes 32-bit value to the Monitor mailbox
*
*/
void write_Monitor_mailbox(long value)
{
  volatile int x;

  do{
    get_semaphore(Mon_mailbox_semaphore);
    x = Mon_MAILBOX->REQ;           /* Poll till mailbox empty */
    release_semaphore(Mon_mailbox_semaphore);
  }while(x);
```

```
  get_semaphore(Mon_mailbox_semaphore);
        /* Update transmit mailbox */
  Mon_MAILBOX->XMT = (long)value;
  Mon_MAILBOX->REQ = -1;
  release_semaphore(Mon_mailbox_semaphore);
}
```

PERMISSION TO COPY

In presenting this thesis in partial fulfillment of the requirements for a master's degree at Texas Tech University or Texas Tech University Health Sciences Center, I agree that the Library and my major department shall make it freely available for research purposes. Permission to copy this thesis for scholarly purposes may be granted by the Director of the Library or my major professor. It is understood that any copying or publication of this thesis for financial gain shall not be allowed without my further written permission and that any user may be liable for copyright infringement.

Agree (Permission is granted.)

Mont Ellis — 1-1-92

Student's Signature — Date

Disagree (Permission is not granted.)

Student's Signature — Date